10 Mixing in food processing

C.D. RIELLY

Introduction

Mixing is fundamental to food processing operations, such as in the preparation of ingredients, the addition of solids to liquids and the development of structure and incorporation of air in the dough mixing process. Chapters 2 and 5 have described the basics of fluid mechanics and of food rheology. Rheology is crucial in mixing; it is obviously more straightforward to mix a fluid such as water than it is to ensure the homogeneity of a highly viscous and non-Newtonian fluid such as a starch solution.

This chapter describes the types of equipment used to carry out a number of different types of mixing process and the principles used to define the extent of mixing. Different types of system are required for the different requirements of the food industry, for example:

- **gas–liquid mixing:** ensuring that enough air is mixed into a fermenter liquid to ensure microbial growth is not oxygen-limited;
- **liquid–liquid mixing:** the creation of liquid–liquid emulsions is central to the manufacture of margarines and spreads;
- **solid–liquid mixing:** the addition of solids to liquids is involved in the reconstitution of fluids, such as when tea or coffee solids are added to hot water. The addition of liquids to solids is key to the production of many food batters, pastes and doughs.

The ideas of dynamic similarity developed in Chapter 2 are critical here in attempting to scale up mixers; it is important to select the right criteria by which mixers are scaled in practice, otherwise large scale systems may not perform as effectively as would be predicted from small-scale tests.

10.1 Fundamentals of mixing

10.1.1 Mixing processes

Mixing operations occur widely throughout the food processing industries. Mixing is used to bring about a physical or chemical change in the materials

Chemical Engineering for the Food Industry. Edited by P.J. Fryer, D.L. Pyle and C.D. Rielly. Published in 1997 by Blackie A & P, an imprint of Chapman & Hall, London. ISBN 0 412 49500 7

being processed: rates of heat and mass transfer are much improved by agitation; the energy input through mixing may be used to blend materials, giving new physical and rheological properties; agitation may be used to disperse multiphase or multicomponent mixtures, prior to further processing or packaging; and chemical reaction rates may be increased by ensuring that the reactants are well mixed and in intimate contact. An application that is peculiar to the food industry is the development of structure by the action of mixing: for example, in dough making, shear and extensional forces generated by the mixer may be used to develop the flour and water into a viscoelastic protein matrix that is capable of retaining the gas produced during proving and baking. Other examples of structured fluids produced by mixing are creams, butters and margarines; in each of these materials the flow field generated by the mixer is used to disperse one liquid phase in another and so form a stable emulsion, which has the required physical, rheological and organoleptic properties.

This chapter follows the conventional chemical engineering approach of identifying similar physical processes and studying them in a unified manner: the processes described here are liquid blending, gas–liquid dispersion, emulsification, solids suspension and dissolution. Qualitative descriptions of mixing mechanisms are presented, along with a discussion of design methods; in many operations the design methods are only approximate and caution should always be exercised in applying these techniques. The discussion in 10.1.2 is equally applicable to either fluid or solids mixtures. The discussion in subsequent sections concentrates on fluid-mixing processes, although solid–solid mixers are described in section 10.10.

10.1.2 The importance of the scale of scrutiny

Assessment of the quality of any mixture depends on how closely the mixture is scrutinized. Consider Fig. 10.1, which shows a mixture of black and white particles, regularly arranged. The first grey square appears well mixed and homogeneous, but as it is increasingly magnified, distinct regions of black and white appear. At each magnification stage a smaller volume of the mixture is scrutinized, until the mixture appears completely segregated. In the last square, at the highest magnification (the smallest scale of scrutiny is of the order of the particle size) the mixture appears to be completely segregated: the composition varies from point to point, but not in a smooth manner. Clearly, any definition of 'mixedness' needs to include a statement about the scale on which the mixture is examined and this in turn must depend on the end use for that mixture.

Danckwerts (1953) defined the scale of scrutiny of a mixture as 'the maximum size of regions of segregation which would cause it to be regarded as unmixed'. For instance, in production of home cake mixes, the proportion of ingredients should be the same in each packet: that is, the important

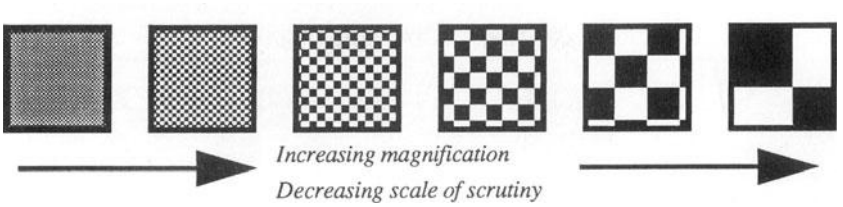

Fig. 10.1 The effect on the mixture appearance of changing the scale of scrutiny.

scale of scrutiny is the size of one packet, and there is no need to ensure homogeneity at a smaller scale. However, when the customer bakes a cake from such a packet, the contents must be mixed on a much finer scale, so that differences in texture or composition cannot be detected by the palate. The scale of scrutiny in the latter case is of the order of one mouthful, but probably less since chemical reactions during baking depend on the homogeneity of the mixture.

The cake mix is an example of a coarse-grained mixture, which consists of a randomization of particles, each of which may be distinguished by the eye. In fine-grain mixtures (such as smoke in air, or a mixture of miscible liquids, such as sugar syrups in water) the composition appears to vary smoothly from point to point. Here, two quantities are required to describe the mixture: the scale of segregation and the intensity of segregation. The **scale of segregation** is a measure of the size of 'clumps' of unmixed components in an imperfect mixture, while the **intensity of segregation** is a measure of the difference in composition from the mean, averaged over all points in the mixture. The latter does not depend on the size of the 'clumps' but rather on the extent to which interdiffusion between components of the mixture has taken place. Figure 10.2 shows schematically the effect of changing the scale and intensity of segregation. As the scale of segregation decreases, the size of the dark regions is reduced; however, as the intensity of segregation decreases, the mixture becomes increasingly diffuse. As the perfectly mixed state is approached both of these quantities tend towards zero. The degree to which these two parameters must be reduced depends on the required scale of scrutiny of the mixture, which in turn depends on the end use for that mixture. It will be seen in the following sections that where diffusional processes are slow or do not exist, then the mixer should be designed to reduce the length scale of segregation to an acceptably small level (for example, in laminar mixing or with coarse solids). In this case the mixture remains segregated at a scale of scrutiny less than the length scale of segregation.

Danckwerts (1953) formally defined the scale and intensity of segregation for a mixture of components A and B in terms of their average and root mean square fluctuating concentrations and correlation functions. In prac-

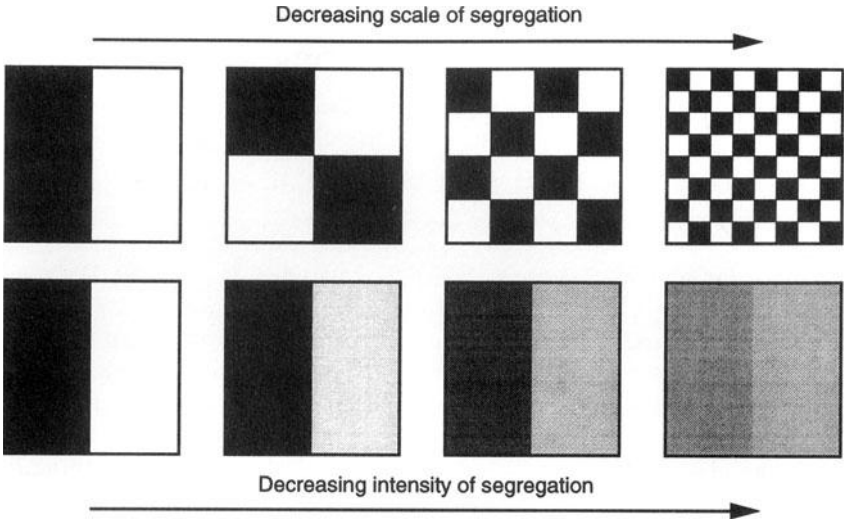

Fig. 10.2 The effects of scale and intensity of segregation on mixedness (adapted from Poux *et al.*, 1991).

tice these quantities are not easy to measure as they require concentration data from a large number of points within the mixture. However, they do provide a sound basis for describing the quality of a mixture and are useful concepts for understanding the way in which fluid or solid mixtures approach a state of homogeneity.

10.1.3 Flow regimes for fluid mixer operations

The flow regimes for fluid mixing may be divided into **laminar** and **turbulent** regions. In a stirred tank, this depends on the impeller Reynolds number, defined as

$$Re = \frac{\rho_L N D^2}{\mu_L} \tag{10.1}$$

In equation (10.1), N is the impeller speed (revolutions per second), D is the impeller diameter, ρ_L is the liquid density and μ_L is the viscosity. In both of these regimes mixing takes place by convective transport of material throughout the mixer and by high shear dispersion in local regions of the mixer close to the moving blades. In the turbulent regime, mixing rates are much enhanced by turbulent diffusion. Molecular diffusion also operates in both regimes and is ultimately responsible for molecular scale homogeneity: that is, at a length scale very much smaller than the typical scale of scrutiny. Molecular diffusion is a slow process, even in low-viscosity sys-

tems, and is only effective over very long times, or at very short length scales. In studies of macro-mixing phenomena (mixing at length scales very much larger than the molecular scale) it is often legitimate to ignore the effects of molecular diffusion, except close to the point of 'perfect' homogeneity.

10.1.4 Laminar mixing mechanisms

The fully laminar flow regime is usually restricted to impeller Reynolds numbers, $Re < 10$. Under typical operating conditions this can only be achieved using liquids with viscosities greater than about 10 Pa s.

In low Reynolds number flows, viscous effects dominate over inertial effects so, to provide adequate agitation, the impeller should sweep through as much of the vessel volume as possible. The regions close to the moving blade have large velocity gradients and high shear rates, where stretching and elongation of fluid elements takes place (see Figs 10.3 and 10.4). Con-

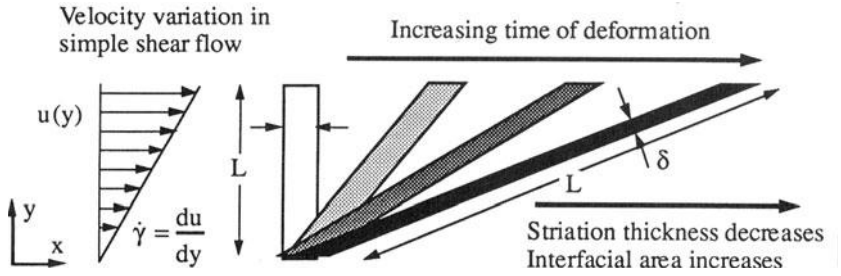

Fig. 10.3 Thinning of fluid elements in a simple laminar shear flow. The initial element is shown in white; the deformed element, at later times, is shown with an increasing depth of grey. The thickness of the element is progressively reduced, whereas its interfacial area (or length) increases with increasing time.

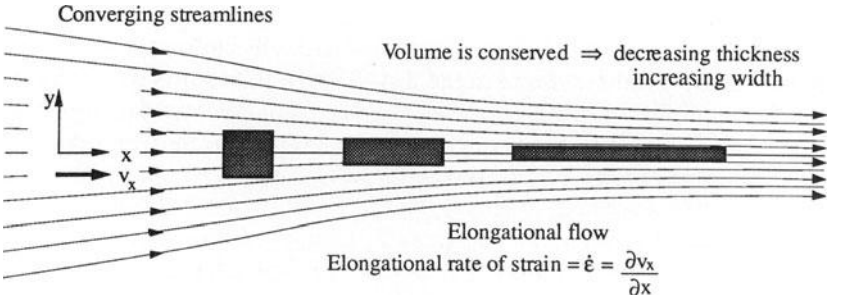

Fig. 10.4 Thinning of fluid elements in an extensional (accelerating) flow.

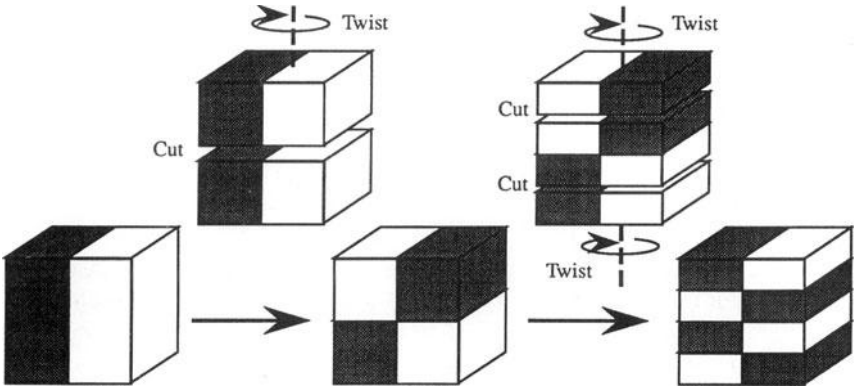

Fig. 10.5 Distributive mixing by repeated cutting and twisting operations.

sider the deformation of a shaded fluid element in these simple flow fields. With increasing duration within the shear or elongational flow the thickness of the element decreases and the material becomes better mixed. If the effects of molecular diffusion are ignored, then the 'interface' between the shaded fluid and the bulk remains sharp. The change in this interfacial area or in the thickness of the element (the striation thickness) may be used as a measure of the degree of mixing that has been achieved.

These effects are most intense near the blades of the mixer. The distorted fluid elements are convected into the bulk flow, where they are reoriented before passing once more through the region of high shear or accelerated flow. The continual process of stretching and thinning, followed by convective mixing and reorientation in the bulk, gradually reduces the striation thickness of fluid elements and increases the homogeneity of the tank contents. Molecular diffusion is required to bring about homogeneity on a molecular scale, but this is a very slow process in viscous liquids and typically the criterion for mixer design is to reduce average striation thickness until inhomogeneities are not visible at the required scale of scrutiny.

In some laminar mixers (such as static mixers, discussed more fully in section 10.9), the mixer blades or elements physically cut and twist the fluid elements and reorientate them in the flow. Figure 10.5 shows the effect of a series of repetitions of these processes: each cutting and rotating operation reduces the striation thickness or scale of segregation, until the required degree of homogeneity is achieved.

10.1.5 Turbulent mixing mechanisms

At high impeller Reynolds numbers, typically $Re > 10^4$, the flow is fully turbulent. Under these conditions inertial effects predominate over viscous

effects and the fluid can be pumped by a small diameter impeller to all regions of the tank. A feature of turbulent flow is that transport processes are much enhanced by turbulent eddy diffusion: that is, turbulent velocity fluctuations give much larger mass, heat and momentum transfer rates than for molecular diffusion alone.

Turbulence is not distributed uniformly throughout the vessel; regions close to the impeller have high turbulent energy dissipation rates and hence high values of the turbulent eddy diffusivity. Thus rapid mixing takes place close to the impeller, while less intense mixing occurs in the bulk flow owing to the combined effects of convection, steady shear and turbulent and molecular diffusion. Effective mixers must provide a rapid turnover of the tank contents, so that fluid elements frequently spend time in the regions of intense agitation, where their scale and intensity of segregation are rapidly reduced. The smallest turbulent motions in a stirred tank have length scales (typically of the order of 10μm) much larger than the molecular scale and thus molecular diffusion is still necessary for ultimate homogeneity. In reacting systems the interaction between turbulent mixing and molecular diffusion is important, as molecules of the reacting species must be intimately mixed for significant reaction rates to be achieved. Furthermore, the relative rates of mixing near the molecular scale and chemical kinetics can affect the selectivity of certain reactions.

In both laminar and turbulent regimes there is an input of energy to the liquid that generates flow and mixing and is eventually dissipated as heat by the action of viscosity. The next section describes design methods for estimating the power requirements for mixing.

10.2 Fluid-mixing equipment

10.2.1 Standard geometry stirred tanks

Low-viscosity applications. In chemical processing and particularly in the food industry there is no such thing as a **standard geometry stirred tank**; however, most design information, from experimental studies and plant-scale measurements, exists for the range of geometries given in Table 10.1. Figure 10.6 shows the geometry of stirred tanks and defines the important dimensions. Much research has been carried out on flat-bottomed tanks, despite the fact that the majority of industrial vessels have dished ends (ellipsoidal or torispherical) for ease of fabrication, cleaning and operation at elevated pressures.

Any design engineer would be well advised to work within these ranges, unless there is a specific process requirement that demands a change from the standard design.

Table 10.1 Standard geometric ratios for stirred tanks (low viscosity applications)

Geometric ratio	Typical range of values	Standard geometry
$\frac{H}{T}$	1–3	1
$\frac{D}{T}$	$\frac{1}{4}-\frac{2}{3}$	$\frac{1}{3}$
$\frac{C}{T}$	$\frac{1}{4}-\frac{1}{2}$	$\frac{1}{3}$
$\frac{C}{D}$	~1	1
$\frac{B}{T}$	$\frac{1}{12}-\frac{1}{10}$	$\frac{1}{10}$

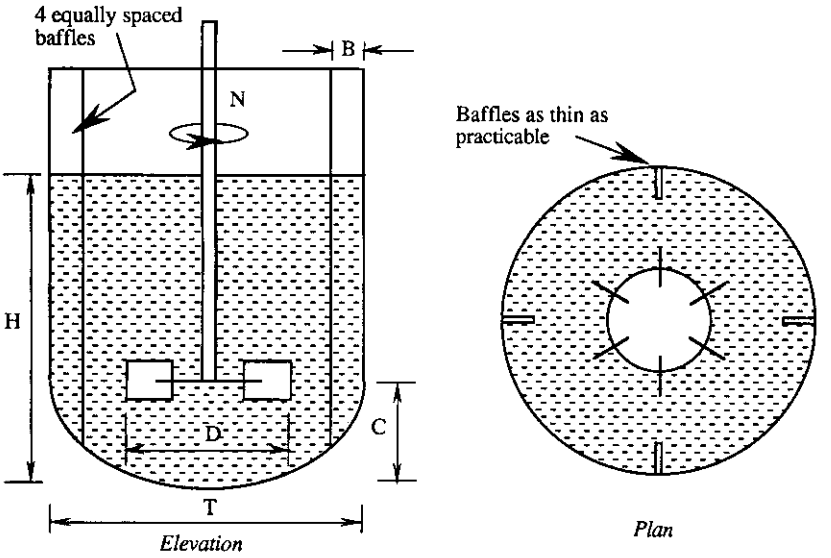

Fig. 10.6 Standard geometry stirred tank (low-viscosity applications).

The tanks may be baffled or unbaffled. More effective mixing is obtained by placing baffles on the tank wall, which generate large axial and radial velocities rather than a purely swirling flow. Full baffling may be achieved using four vertical baffles mounted radially, 90° apart; the baffles should extend to at least the free surface but often have a small clearance from the

base of the vessel. For fluid mixing with dispersed solid particles, the baffles may be supported off the wall, leaving a gap of $\sim T/14$. This is designed to prevent build-up of particles in the crevice between the baffles and the wall and to facilitate cleaning. In the food industry, prismatic baffles (with triangular cross-section) with flush welds are often used to eliminated build-up of residues in corners and for ease of cleaning and sterilization.

In low-viscosity liquids, small-diameter impellers (small D/T ratios) are able to generate flow in all parts of the tank at moderate power inputs. The common impeller types are shown in Fig. 10.7; they can be classed according to the type of discharge flow produced (see section 10.2.2 for further details).

Impeller flow type	**Examples**
Radial	flat paddle, disc turbine
Axial	marine propeller
Axial and radial mixed flow	pitched blade turbine, hydrofoil

With aspect ratios (H/T) greater than about 1.5 it is usual to have multiple impellers on the same shaft (each a distance of ~ 1–$2D$ apart) to give

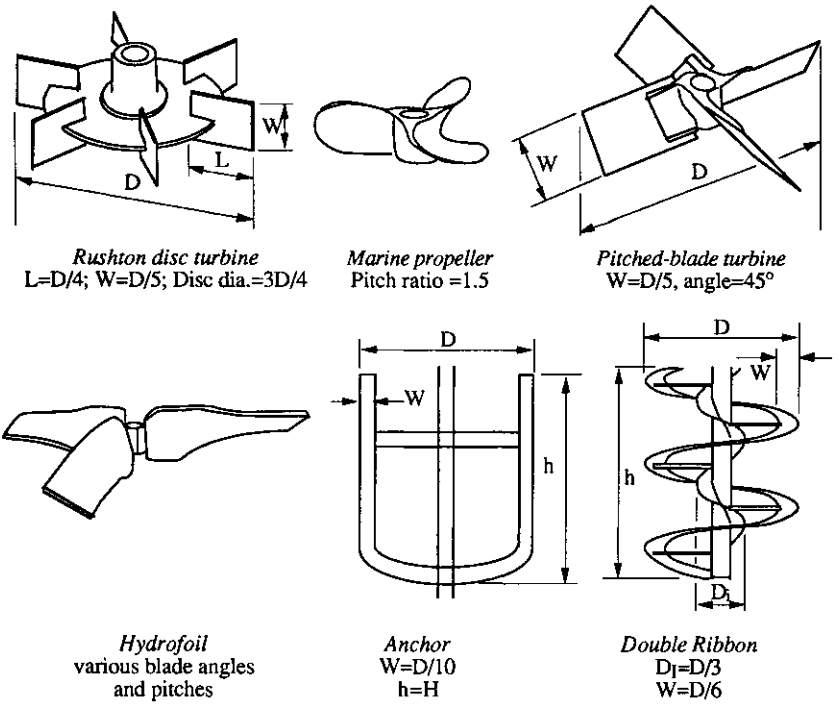

Fig. 10.7 Standard geometries for common impeller types.

effective agitation throughout the tank volume. These impellers also have standard geometry designs: for example, a typical width to diameter ratio, W/D, of 1/5 for Rushton disc turbines and mixed-flow pitched-bladed turbines. The standard geometries for a number of common impeller types are shown in Fig. 10.7. A large number of literature measurements have been made on the standard Rushton disc turbine (six-bladed). Formerly this design was regarded as one of the best multipurpose agitators; however, recent research has shown that hydrofoil or pitched-bladed impellers have certain advantages for specific low-viscosity operations (see section 10.2.2). Marine propellers (three-bladed) are also much used, operating at high rotational speeds with low D/T ratios. No 'standard' propeller design has emerged, because of the variety of blade shapes, blade sections and pitch ratios available. For all these designs the typical impeller tip speed would be about $3\,m\,s^{-1}$ and certainly no more than $4–5\,m\,s^{-1}$. High tip speeds cause shear damage to sensitive particulates, cells and structured fluids.

High-viscosity applications. A great variety of tank and impeller designs are available to suit specific requirements for agitating high-viscosity liquids. Small-diameter impellers, described in the previous section, are only suitable for liquids with viscosities up to 2 Pa s for propellers and 50 Pa s for turbines (Edwards, 1985).

At high viscosities, small impellers only generate significant flows in the vicinity of the blades and are wasteful in their use of power compared with large-diameter paddles. Anchors and helical ribbon impellers are used, which have close clearances between the blades and the wall, and sweep through a large volume of the tank. These features are designed to prevent

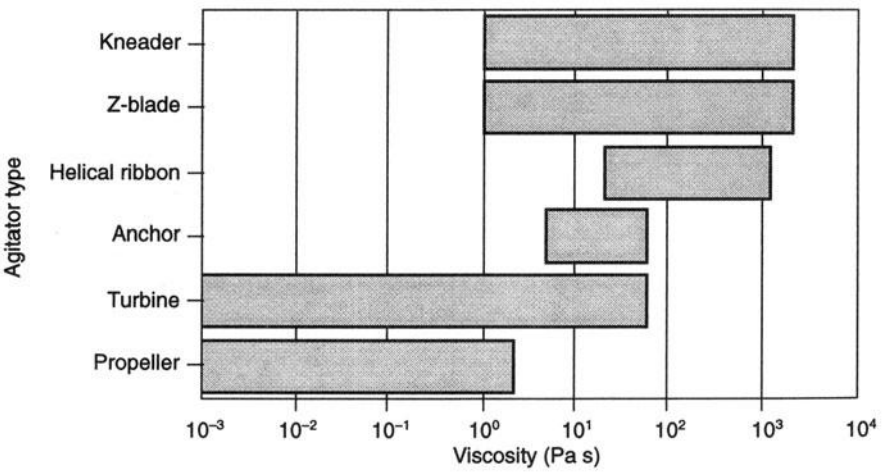

Fig. 10.8 Mixer selection chart for fluid processing.

the formation of stagnant zones within the fluid. Some typical geometries for anchor impellers and helical ribbons are also shown in Fig. 10.7. With viscous liquids these tanks are often unbaffled, as gross vortexing is not a problem. For very high-viscosity mixing applications ($\mu > 1000$ Pa s) ribbons are unsuitable and kneaders, Z or sigma blade mixers are used (see section 10.9). Figure 10.8 summarizes this information in a selection chart for mixer types as a function of the viscosity of the fluid to be agitated.

10.2.2 Flow patterns

All small-diameter impellers, rotating at high speed in low-viscosity liquids, in **unbaffled** tanks produce a predominantly tangential swirling flow, with weaker, secondary vertical circulations. Nagata (1975, Ch. 3) presents velocity profiles for a variety of impellers in unbaffled tanks and (Ch. 1) describes a theoretical model for the flow, consisting of a central solid body (forced vortex) region with an outer free vortex. For a full description of forced and free vortex motion see Kay and Nedderman (1985, Ch. 3) Clearly, in the central, solid-body rotation (see Fig. 10.9) there is no relative movement of fluid elements and hence no mixing; in the outer region mixing is only achieved in the tangential direction (secondary vertical circulations, which are not included in the analysis, do not contribute significantly to mixing). At higher impeller speeds the surface vortex extends to the impeller blades and air is entrained. Consequently, unbaffled tanks are not efficient for blending operations. Use of an eccentric impeller improves blending efficiency by preventing the formation of the forced vortex, but

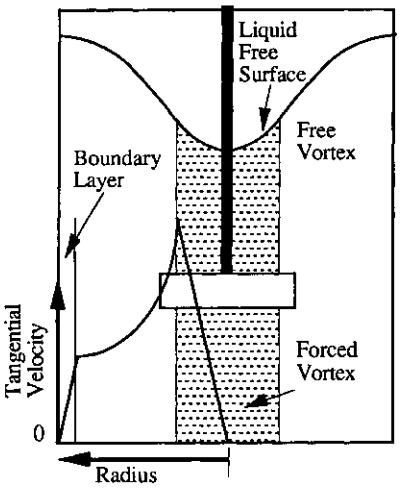

Fig. 10.9 Forced/free vortex rotation in an unbaffled tank.

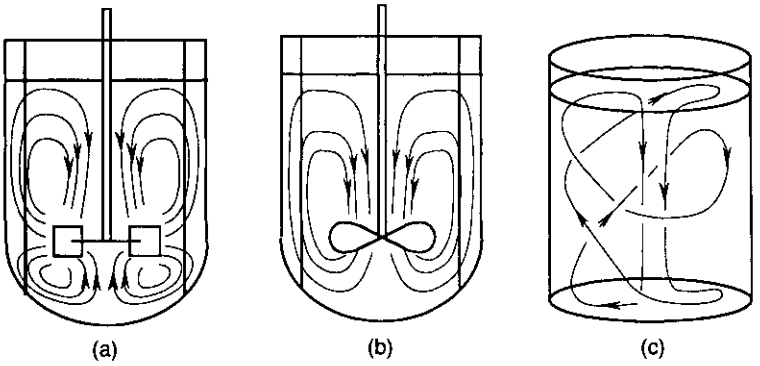

Fig. 10.10 Flow patterns for common impeller types: (a) radial flow pattern (low-viscosity liquids); (b) axial flow pattern by marine impeller (low-viscosity liquids); (c) flow pattern by ribbon mixer (high-viscosity liquids).

also introduces an additional problem that air is entrained from the free surface at low impeller speeds. In some food processes air entrainment is undesirable, as oxidation of vitamins and spoilage may occur during product storage.

Baffling redirects the tangential and radial flow in the impeller discharge stream, generating strong vertical circulations. In baffled tanks, two distinct types of flow may be identified: (a) **radial flow**, as produced by the Rushton disc turbine; and (b) **axial flow**, as produced by the marine propeller. Pitched-bladed turbines generate a **mixed** flow with both axial and radial components in the discharge stream. These common flow patterns are illustrated in Fig. 10.10 (note that there is an additional tangential velocity superimposed on these flows). In addition, these flows exhibit a pseudo-periodicity due to shedding of trailing vortices from the impeller blades; that is, there is an element of unsteadiness in the flows. Clearly these extremely complex, three-dimensional flows are difficult to model theoretically, and so many results are based on experimental observations and simplified physical models.

More modern impeller designs (such as the hydrofoil impeller shown in Fig. 10.7) give various combinations of axial and radial flow, depending on blade shape and pitch. In applications such as blending or particle suspension, the impeller should produce a strong circulating flow, but consume only a small amount of power. In contrast, in gas–liquid or liquid–liquid dispersions high rates of energy dissipation are required to break up droplets or bubbles (see sections 10.5 and 10.6). Recent interest has focused on the distribution of energy dissipation within the tank: the energy input through the shaft is not dissipated uniformly throughout the tank. For example, the radial disc turbine has a high power input and also has high

rates of energy dissipation in the vicinity of the impeller and low dissipation rates in the bulk flow. It will be seen in the following sections that this implies intense mixing in the impeller regions but more gentle mixing elsewhere. By comparison, modern hydrofoil impellers produce strong liquid circulations, yet have a low overall power input and dissipate this energy more uniformly throughout the tank volume. Therefore these types of impeller show some advantages for solids suspension and liquid blending.

When anchor impellers or helical ribbons are used in high-viscosity liquids, the fluid flow patterns are very different from those for small diameter impellers: compare the diagrams in Fig. 10.10. Large-diameter impellers attempt to generate flow throughout the whole tank and eliminate stagnant zones. Anchors are often used for heat transfer applications or to scrape sticky materials off the wall, but are not recommended for liquid blending (see section 10.4.3) as they produce only weak vertical circulations. Ribbon mixers (see Figs 10.7 and 10.10) give strong flows in the radial and axial directions, and are preferred for mixing of miscible liquids.

Mixing in low-viscosity systems is determined by the amount of turbulence and rate of circulation generated by the impeller. The intensity of turbulence within the flow depends on the power input of the impeller (discussed in the next section). The circulation rate depends on the pumping capacity of the impeller. Many authors have calculated impeller discharge flowrates, Q_L, from velocity measurements in the vicinity of the blades (e.g. Nagata, 1975, Ch. 3). Their results are presented in dimensionless form as a flow coefficient N_Q (analogous to the discharge coefficient for a centrifugal pump) versus the impeller Reynolds number (defined in equation (10.1)):

$$N_Q = \frac{Q_L}{ND^3} = f(Re) \tag{10.2}$$

For low-viscosity fluids the flow is usually turbulent ($Re > 10^4$) and the flow coefficient is a constant, independent of impeller speed and diameter, so that the discharge flow rate is directly proportional to ND^3. Revill (1982) recommends that for standard geometry disc turbines

$$N_Q = \frac{Q_L}{ND^3} = 0.75 \qquad \text{for} \qquad 0.2 < \frac{D}{T} < 0.5 \tag{10.3}$$

Uhl and Gray (1966, Vol. 1, Ch. 4) also present a large number of flow coefficients, N_Q, for various impellers in baffled and unbaffled vessels. The concept of the discharge flow gives a good qualitative indication of the impeller's ability to generate fluid motion, but is not particularly useful in the design of mixing systems, unless it can be directly linked to blend times or solids suspension criteria (examples of this are provided by Joshi *et al.*, 1982). Moreover, as the discharge stream leaving the impeller entrains

other fluid from the bulk flow, Q_L is **not** the same as the circulation flow within the vessel.

10.3 Power consumption in stirred tanks

10.3.1 Single Newtonian liquid phase: dimensional analysis

Calculation of the power input by agitation is of fundamental importance to both the process and mechanical design of stirred tanks. As described in section 10.2, the fluid dynamics of stirred tanks is so complex as to preclude an a priori calculation of power input for a given impeller speed. In such cases, dimensional analysis may be used to indicate the form of the relationship between power and impeller rotational speed.

The power input P_o through a rotating impeller is a function of impeller speed N, impeller diameter D, liquid density ρ_L and viscosity μ_L, gravitational acceleration g, and the tank geometry (see Fig. 10.6). The subscript 'o' is used to indicate the power input in the absence of gas sparging: that is, for a single liquid phase. By convention the impeller speed is measured in revolutions per second (rps) rather than radian s^{-1}.

$$P_o = f_1\big(N,\ D,\ \rho_L, \mu_L,\ g,\ T,\ H,\ C,\ B,\ \ldots,\ \text{impeller type and geometry}\big) \tag{10.4}$$

Forming dimensionless groups using Buckingham's theorem:

$$\frac{P_o}{\rho_L N^3 D^5} = f_2\left(\frac{\rho_L N D^2}{\mu_L},\ \frac{N^2 D}{g},\ \frac{D}{T},\ \frac{H}{T},\ \frac{C}{D},\ \frac{B}{T}\right) \tag{10.5}$$

Define

$$N_{po} = \frac{P_o}{\rho_L N^3 D^5} = \text{ungassed power number} \tag{10.6}$$

$$Re = \frac{\rho_L N D^2}{\mu_L} = \text{Reynolds number} \tag{10.1}$$

$$Fr = \frac{N^2 D}{g} = \text{Froude number} \tag{10.7}$$

Note that the Reynolds and Froude numbers reduce to their familiar forms (Chapter 2)

$$Re = \frac{\rho_L v_L}{\mu_L} \qquad \text{and} \qquad Fr = \frac{v^2}{gL}$$

where $v = ND$ is a characteristic velocity (related to tip speed) and $L = D$ is a characteristic length.

In geometrically similar systems (ratios of geometric dimensions are equal but the scales are different), the power number depends only on the Reynolds and Froude numbers:

$$N_{po} = f_3(Re, Fr) \tag{10.8}$$

Furthermore, for stirred tanks in which the liquid surface is relatively flat (such as baffled systems) the gravitational acceleration has a negligible effect on power demand, and so

$$N_{po} = f_4(Re) \tag{10.9}$$

Unbaffled systems, in which a central vortex forms, retain the general dependence of the power number on the Froude number (equation (10.8)), although the influence of the Reynolds number is predominant. This is because gravitational acceleration affects the formation of the surface vortex.

A complete power characteristic for various impeller types is presented in Fig. 10.11. At low Reynolds numbers there is no difference in the N_{po}–Re relationship between unbaffled and baffled systems using the same impeller. However, at high Reynolds numbers (transitional and turbulent flow), baffled systems draw considerably more power than unbaffled, indicating higher intensities of turbulence and improved mixing rates.

The power number can be shown to be analogous to a drag coefficient for the rotating impeller blades (Uhl and Gray, 1966, Vol. 1, Ch. 4). Therefore, it is not surprising that for laminar flows ($Re < 10$) the power number is inversely proportional to the Reynolds number: that is, equation (10.9) becomes

$$N_{po} = \frac{A}{Re} \tag{10.10}$$

where A is a constant that depends on impeller type. Edwards and Ayazi-Shamlou (1983) presented the following correlations for laminar flows, which allow for variations in impeller geometry:

Helical ribbon

$$N_{po} = \frac{150}{Re}\left(\frac{C}{D}\right)^{-0.28}\left(\frac{p}{D}\right)^{-0.53}\left(\frac{h}{D}\right)\left(\frac{W}{D}\right)^{0.33} n_b^{0.54} \tag{10.11}$$

Anchor

$$N_{po} = \frac{85}{Re}\left(\frac{C}{T}\right)^{-0.31}\left(\frac{h}{D}\right)^{0.48} \tag{10.12}$$

where C is the clearance to the wall, D is the outside diameter of the impeller, p is the pitch, h is the height of the impeller, W is the blade width and n_b is the number of blades.

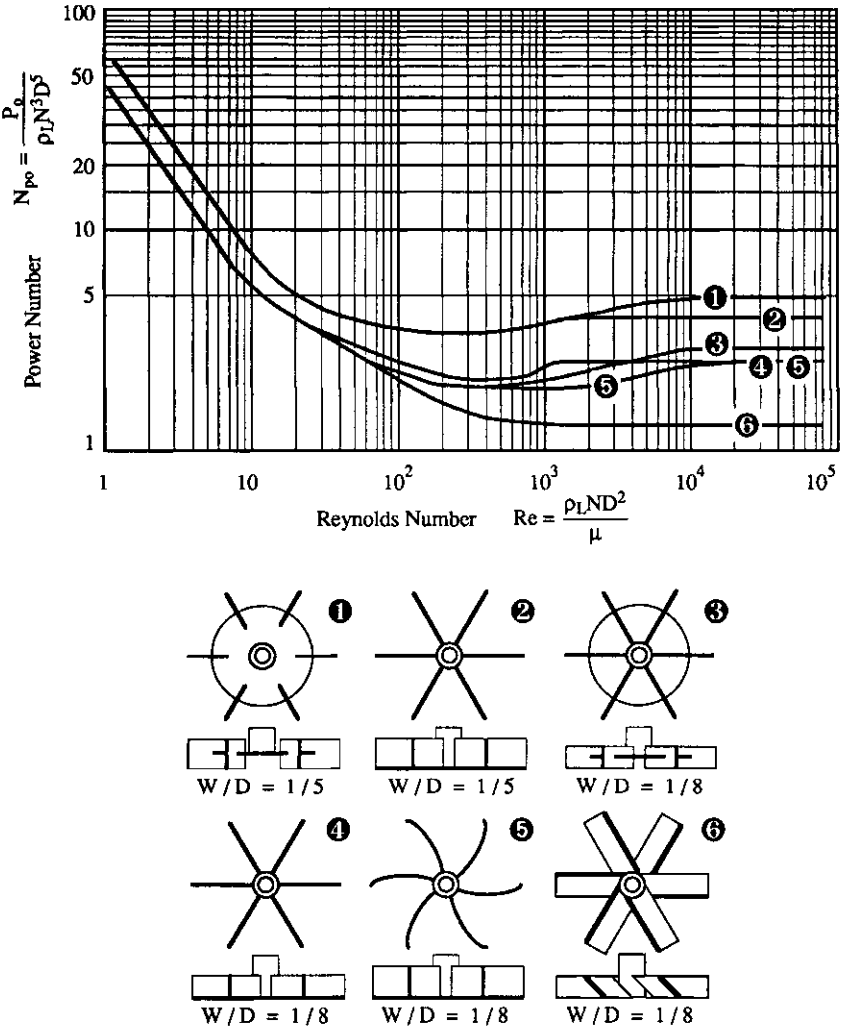

Fig. 10.11 Power characteristics for various impeller types in baffled tanks.

At high Reynolds numbers ($Re > 10^4$) the flow is turbulent, and the power number is a constant that depends only on impeller type and tank geometry:

$$N_{po} = \Phi = \text{constant} \tag{10.13}$$

Values of the constant power number Φ for common impeller types are presented in Table 10.2 (see also Uhl and Gray, 1966, Vol. I, Ch. 3).

In the transition regime, few correlations exist for the N_{po}–Re relationship, and most results are presented graphically. Nagata (1975, Ch. 1)

Table 10.2 Constant power numbers for various standard impellers (Bates *et al.*, 1963) (n_b is the number of blades and n_B is the number of baffles)

Turbine	$\frac{D}{W}$	n_b	$\frac{D}{T}$	$\frac{C}{T}$	n_B	$\frac{B}{T}$	Φ
Flat blade	0.125	6	0.33	0.33	4	0.083	2.6
Flat blade	0.20	6	0.33	0.33	4	0.083	4.0
Rushton disc turbine ($L/D = 0.25$)	0.20	6	0.33	0.33	4	0.10	5.0
Rushton disc turbine ($L/D = 0.5$)	0.125	6	0.33	0.33	4	0.083	3.0
Curved blade	0.125	6	0.33	0.33	4	0.083	2.6
45° Pitched blade	0.125	6	0.33	0.33	4	0.083	1.3

combines the forms of equations (10.10) and (10.13) for the transition regime as

$$N_{po} = \frac{A}{Re} + B \tag{10.14}$$

and gives expressions for the constants A and B in terms of impeller and tank geometric ratios.

10.3.2 Non-Newtonian liquids

The power input to a non-Newtonian liquid may be estimated, based on an 'apparent' viscosity μ_a (Metzner and Otto, 1957). This method assumes that there is a representative 'average shear rate' $\dot{\gamma}$, which, by dimensional analysis, should depend only on the impeller speed (for a given impeller type and fixed geometry at any scale):

$$\dot{\gamma} = \beta N \tag{10.15}$$

where β is a dimensionless shear rate constant. For a power-law fluid (Chapter 5) the shear stress is

$$\tau = K\dot{\gamma}^n \tag{10.16}$$

where K is the consistency index and n is the power-law exponent, or

$$\mu_a = \frac{\tau}{\dot{\gamma}} = K\dot{\gamma}^{n-1} \tag{10.17}$$

From equations (10.15) and (10.17):

$$\mu_a = K(\beta N)^{n-1} \tag{10.18}$$

and the Reynolds number (see equation (10.1)) becomes

$$Re = \frac{\rho_L N D^2}{\mu_a} = \frac{\rho_L D^2}{K\beta^{n-1} N^{n-2}} \tag{10.19}$$

Metzner and Otto (1957) demonstrated that the relationship of Newtonian power number to Reynolds number also held for non-Newtonian fluids,

Table 10.3 Dimensionless shear rate constants for pseudo-plastic liquids

Impeller	Shear rate constant, β	Source
Six-bladed disc turbine	11.5 ± 1.5	Metzner and Otto (1957)
Six-bladed 45° pitched turbine	13 ± 2	Metzner and Otto (1957)
Marine propeller	10 ± 0.9	Metzner and Otto (1957)
Helical ribbon	$34 - 114\left(\frac{C}{D}\right)$ for $0.026 < \left(\frac{C}{D}\right) < 0.164$	Edwards and Shamlou (1983)
Anchor	$33 - 172\left(\frac{C}{T}\right)$ for $0.02 < \left(\frac{C}{T}\right) < 0.13$	Edwards and Shamlou (1983)

defining the Reynolds number using equation (10.19). Values for the shear rate constant β for shear-thinning fluids ($n < 1$) in standard-geometry vessels are presented in Table 10.3 (consult original references for full details of impeller and tank geometries).

To calculate the power input to a non-Newtonian liquid using a standard impeller type the following procedure should be followed.

1. Measure the shear stress versus rate of strain relationship for the non-Newtonian process fluid and fit the constants in equation (10.16) using linear regression of a log–log plot.
2. Calculate the modified Reynolds number from equation (10.19) using the value of the shear rate constant β from Table 10.3, at the required impeller speed.
3. Use an equation or graph for the N_{po}–Re relationship for the same impeller to calculate the power number.
4. Back-calculate the power using the definition of N_{po} in equation (10.6).

Note that an analogous method may be derived for non-Newtonian liquids, which obey different constitutive equations. Calculations for non-standard impellers require measurements of power consumption to be made at a pilot scale using both Newtonian and non-Newtonian fluids, covering the same range of Reynolds numbers as the full-scale design.

10.4 Miscible liquid blending operations

10.4.1 Blending of low-viscosity liquids

A large category of food-mixing operations fall into the category of liquid blending (for example, mixing of sugar syrups, water, fruit pulp and minor ingredients in the manufacture of soft drinks). For low-viscosity Newtonian liquids the process result may be achieved with a small diameter impeller (such as a Rushton turbine, pitched-blade turbine, propeller or hydrofoil),

operated at high speed, but using a fairly low specific power input (typically ~0.2 kW m^{-3}; Edwards, 1985). Usually the flow is in the turbulent regime.

One design requirement is to predict the impeller speed to mix the tank contents, to a given degree of homogeneity, in a given time. Then, for a known impeller speed, tank geometry and fluid properties, the power consumption for mixing can be calculated using the methods in section 10.3. Even for single-phase operations, the fluid flow patterns in a stirred tank are sufficiently complex to preclude an a priori prediction of the mixing time for a given impeller speed. Instead, previous workers have measured mixing times experimentally and used dimensional analysis to correlate their results.

Mixing times may be measured by releasing a tracer liquid into the flow and following the time history of concentration fluctuations; ideally, the tracer liquid should have the same density and viscosity as the bulk liquid. Experimental techniques for measuring the tracer concentration include: visual observation of a coloured dye; light absorption using a dyed tracer; changes of refractive index; temperature variations of a hot or cold tracer; acid–base reactions using a coloured pH indicator; and conductivity using a salt tracer. Figure 10.12 shows the dimensionless tracer concentration c^* as a function of time from release of the tracer. These results were measured using a sodium chloride tracer, which was detected by a microconductivity probe located in the discharge stream of a Rushton disc turbine. The measured concentration (or conductivity, which is a linear function of concentration) is made dimensionless using the initial tracer concentration in

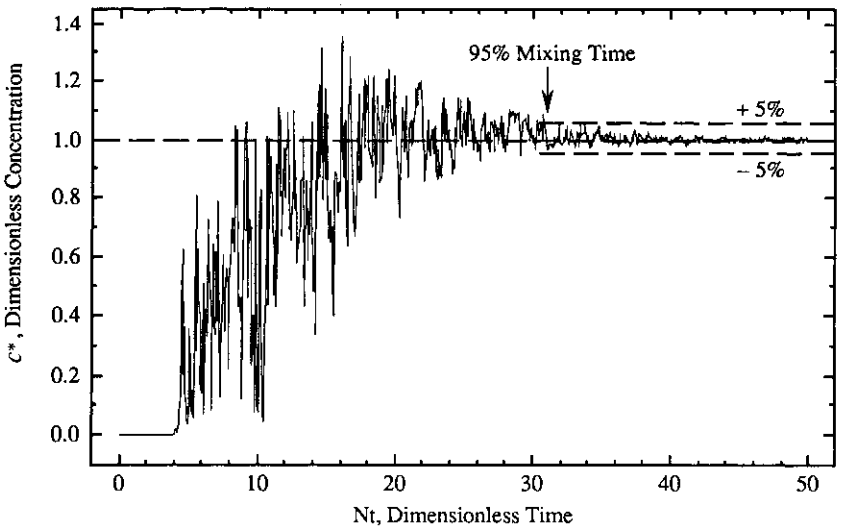

Fig. 10.12 Concentration time history.

the tank before the start of the experiment, c_0, (usually zero) and the final tank concentration, c_∞, when the contents are fully mixed.

$$c^* = \frac{c(t) - c_0}{c_\infty - c_0} \tag{10.20}$$

That is,

$$c^*(t = 0) = 0 \qquad \text{and} \qquad c^*(t \to \infty) = 1$$

Time may be made dimensionless by defining

$$t^* = Nt \tag{10.21}$$

A 95% mixing time, θ_{95}, may be defined as the time for the concentration to fall within ±5% of the final concentration. That is,

$$0.95 \leqslant c^* \leqslant 1.05 \qquad \text{for all } t \geqslant \theta_{95}$$

Similarly 90% and 99% mixing times may be defined, 99% implying a greater degree of homogeneity than 95% and consequently a longer mixing time; for most practical purposes a 95% mixing time is sufficient. Rielly and Pandit (1988) demonstrated that the mixing time is independent of the position of the detection device for fairly stringent criteria of mixedness, such as 95%; a mass balance applied to any element of the flow shows that as the mixedness criterion approaches 100%, mixing times measured at any position within the tank should be equal.

If simultaneous measurements of the tracer concentration can be made at several positions in the tank, a mixing time can be defined in terms of the decrease in concentration variance. For n detectors the variance σ^2 is defined by

$$\sigma^2(t) = \frac{1}{n-1} \sum_{i=1}^{n} \left(c_i^*(t) - \bar{c}^* \right)^2 \tag{10.22}$$

Note that $\bar{c}^* = 1$ is the tank **average** concentration at all times, $t > 0$ and that $\sigma(t)$ decays with time. The mixing time may defined as the time when $\sigma \leqslant 0.05$ (say). This latter method has the advantage that measurements are taken at many points in the flow and may well show up stagnant regions. However, it is a much more difficult technique to use in practice as it requires recording of many signals simultaneously.

10.4.2 Dimensional analysis of liquid blend times

The previous section shows that several definitions of mixing time are in common use and that they use an arbitrary criterion for mixedness. Whatever definition is used, the mixing time depends on the following parameters:

$$\theta = f_1\left(\rho_L, \mu_L, N, T, D, g, \mathcal{D}, L_d, \begin{matrix}\text{tank and impeller} \\ \text{geometric dimensions}\end{matrix}\right) \tag{10.23}$$

where $\mathcal{D}$ is the liquid molecular diffusion coefficient (m^2s^{-1}) and L_d is the probe resolution length scale (m). The length scale L_d is associated with the scale of scrutiny of the detector and is determined by its physical size and its ability to respond to rapidly fluctuating concentrations. Concentration fluctuations that are much smaller than L_d are not detected and the mixture appears well homogeneous. Many workers omit full details of the scale of scrutiny of their measurement device, making their results unreliable for scale-up. Typically, as the scale of scrutiny of the detector increases, the response to small-scale rapid concentration fluctuations is attenuated and shorter mixing times are measured.

Forming dimensionless groups from equation (10.23):

$$N\theta = f_2\left(\frac{\rho_L N^2 D}{\mu_L}, \frac{ND^2}{g}, \frac{\mu_L}{\rho_L \mathcal{D}}, \frac{T}{D}, \frac{L_d}{T}, \text{ geometric ratios}\right) \tag{10.24}$$

or

$$N\theta = f_2\left(Re,\ Fr,\ Sc,\ \frac{T}{D},\ \text{geometric ratios}\right) \tag{10.25}$$

Here the Reynolds and Froude numbers are given by equations (10.1) and (10.7), and Sc is the **Schmidt number**:

$$Sc = \frac{\mu_L}{\rho_L \mathcal{D}} \tag{10.26}$$

which is the ratio of momentum to mass diffusivity.

For baffled systems, the free surface is relatively flat and the Froude number has a negligible effect on the dimensionless mixing time $N\theta$. However, for unbaffled systems $N\theta$ retains the general dependence of equation (10.25).

The Schmidt number Sc in equation (10.25) includes the effects of the molecular diffusivity $\mathcal{D}$. The smallest practical detectors have a length scale of around 1 mm, yet on these scales molecular effects act only very slowly and hence the Schmidt number may be neglected in the analysis of macromixing phenomena. Moreover, the molecular diffusivities of most solutes in low-viscosity solvents have the same order of magnitude $\mathcal{D} \sim 10^{-9} m^2 s^{-1}$ and Sc of the order of 10^3.

At large Reynolds numbers (low-viscosity, high-speed agitation), $Re > 10^4$, the flow is turbulent and the dimensionless mixing time depends only on the tank geometry and impeller type. Literature reports of scale dependency of $N\theta$ might be attributable to incorrect scaling of the detector scale of scrutiny. Thus

$$N\theta = f_3\left(\text{impeller type, geometric ratios, } \frac{L_d}{T}\right) \tag{10.27}$$

Correlations for constant $N\theta$ values ($Re > 10^4$) for the standard impeller types are given below (Prochazka and Landau, 1961). The disc turbine conformed to the standard geometry, the propeller had a constant pitch equal to diameter, and the pitched-bladed turbine had 4 × 45° blades, with projected height of $0.177D$. The tank geometry was: $H = T$; $B = T/12$; $C = T/2$; $n_B = 4$.
Propeller:

$$N\theta = 3.48\left(\frac{T}{D}\right)^{2.05} \log_{10}\left(\frac{2}{X}\right) \tag{10.28}$$

Pitched-bladed turbine:

$$N\theta = 2.02\left(\frac{T}{D}\right)^{2.20} \log_{10}\left(\frac{2}{X}\right) \tag{10.29}$$

Disc turbine:

$$N\theta = 0.905\left(\frac{T}{D}\right)^{2.57} \log_{10}\left(\frac{2}{X}\right) \tag{10.30}$$

The variable X is the mixedness fraction: for example, $X = 0.05$ for the 95% mixing time.

10.4.3 Blending of viscous liquids

As discussed in section 10.2.2, small-diameter impellers do not give adequate mixing in viscous liquids. Large-diameter impellers, which sweep a large proportion of the tank volume, are used at low speed; typical power inputs are of the order of $2\,kW\,m^{-3}$ (that is, fairly intense agitation, and under normal operating conditions the flow is laminar). Hoogendoorn and den Hartog (1967) showed that for helical ribbons and marine impellers or helical screws in draught tubes, the dimensionless mixing time $N\theta_{75}$ was approximately constant, independent of the impeller speed and liquid viscosity in the laminar regime. The values of $N\theta_{75}$ for disc turbines and anchor impellers were found to decrease with increasing Reynolds number; these authors noted that the latter impellers gave very poor mixing performance at low Reynolds numbers. Nagata (1975, Ch. 4) and Hoogendoorn and den Hartog (1967) reported values of $N\theta_{70} = 33$ and $N\theta_{75} = 65$ respectively for helical ribbon agitators, and found no effect of tank diameter on these values. Figure 10.13 illustrates the dependence of $N\theta_{75}$ on the Reynolds number for viscous fluids with a variety of impellers.

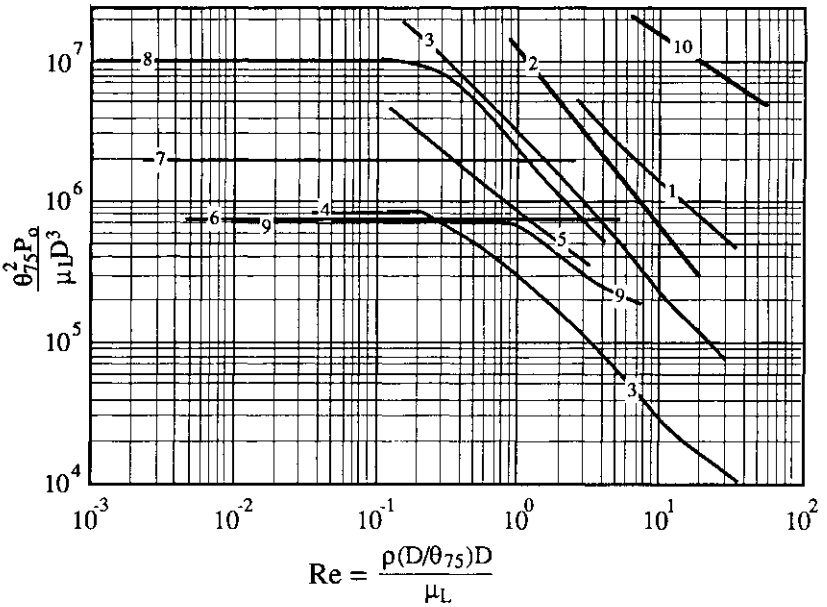

Fig. 10.13 Dimensionless mixing time versus Reynolds number for various impellers in viscous liquids. The tanks were unbaffled, unless otherwise stated. 1, turbine (baffled); 2, turbine; 3, three inclined-blade paddles; 4, three inclined-blade paddles (with draught tube); 5, screw; 6, screw plus draught tube; 7, ribbon; 8, propeller A plus draught tube; 9, propeller B plus draught tube; 10, anchor. (Hoogendorn and den Hartog, 1967).

10.4.4 Problems with blending non-Newtonian liquids

It has already been stated that in viscous liquids the inertia imparted by the impeller is damped out by viscous effects. The flow in regions distant from the blades is weak and mixing is poor. Bingham plastic fluids (Chapter 5, section 5.1.1) can also pose significant mixing problems when agitated by a small-diameter impeller. A cavern of well-mixed (often turbulent) fluid forms in the high-stress regions around the impeller, yet away from the impeller the fluid is stagnant (see Fig. 10.14). The boundary surface of the well-mixed cavern is where the local stress equals the fluid yield stress (recall that there is only shear in a Bingham plastic when the fluid stress exceeds the yield stress). Figure 10.14 shows that as the impeller speed increases, the size of the cavity grows until eventually the whole of the tank contents are well mixed (the usual operating condition). Nienow and Elson (1988) used X-ray flow visualization to reveal the size of cavities in opaque plastic fluids and proposed a model to predict cavity diameter D_c as a function of impeller speed N, power number N_{po} and fluid yield stress τ_y:

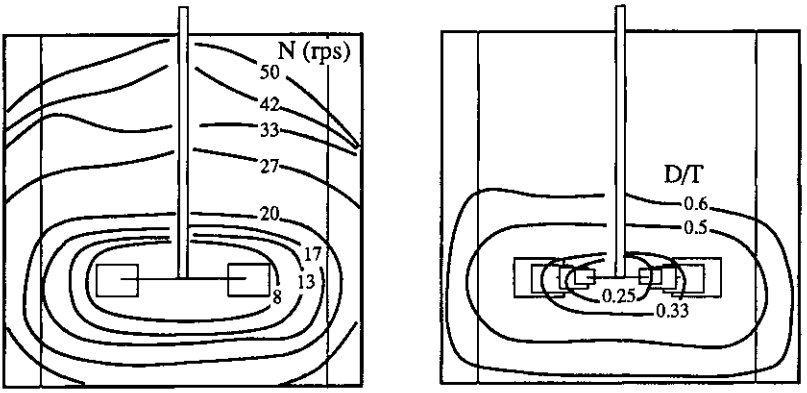

(a) D/T = 0.5 (b) N = 8 rps

Fig. 10.14 Cavern formation in a yield stress fluid (Nienow and Elson, 1988): (a) effect of impeller speed, (b) effect of impeller size on cavern size in xanthan gum.

$$\left(\frac{D_c}{D}\right)^3 = \left(\frac{1.36}{\pi^2}\right)\left(\frac{N_{po}\rho_L N^2 D^2}{\tau_y}\right) \tag{10.31}$$

Here the height of the cylindrical cavity is assumed to be 40% of its diameter. Equation (10.31) allows calculation of the impeller speed to give a cavity equal to the tank diameter, ensuring good mixing throughout the vessel and no dead zones.

Different mixing problems may be found with fluids that exhibit **viscoelastic** behaviour. Elastic effects cause large normal forces to be generated within the fluid, as well as the usual shear forces due to viscous effects. Normal forces oppose the formation of a central vortex around a rotating shaft and can actually cause the fluid to climb. This phenomenon is known as the **Weissenberg effect** and can result in the fluid climbing as high as the shaft seals or gearbox. At low impeller speed these normal forces can also cause flow reversal, i.e. the flow is in the opposite direction to that observed for inelastic fluids at similar Reynolds numbers.

10.5 Gas–liquid mixing

10.5.1 Surface aeration phenomena in stirred tanks

In many food-processing applications it is important to avoid entraining air during the mixing process, as this causes spoilage during product storage. Many workers have noted that in the absence of gas sparging, surface aeration occurs above a minimum impeller speed, denoted by N_{SA}. The forced/free vortex model illustrated in Fig. 10.9 for flow in an unbaffled tank

may be used to predict the point at which the free surface reaches the impeller; typically, for a Rushton turbine the change from forced to free vortex flow occurs at a radius of $3D/8$. Greaves and Kobbacy (1981) gave a qualitative description of the aeration phenomena from the free surface in baffled tanks, at $N > N_{SA}$. Strong eddies (A in Fig. 10.15), formed by the interaction of the discharge flow from the impeller with the baffles, induce other strong eddies (B in Fig. 8.15), which precess slowly around the impeller shaft and form a hollow vortex at the surface. At sufficiently high impeller speeds gas bubbles enter the liquid through the surface vortex B and are carried down to the impeller by the circulating liquid.

Van Dierendonck *et al.* (1968) have correlated N_{SA}, the critical speed for the onset of aeration against physical properties and geometric parameters. Van Dierendonck's correlation for a standard disc turbine in a baffled tank is

$$\left(\frac{\mu_L N_{SA} D^2}{T\sigma}\right)\left(\frac{\rho_L \sigma^3}{g\mu_L^4}\right)^{1/4} = 2.0\left(\frac{H-C}{C}\right)^{1/2} \tag{10.32}$$

which is restricted to

$$0.10 \leqslant \frac{H-C}{T} \leqslant 0.20 + 1.75\frac{D}{T}$$

10.5.2 Aerated impeller power consumption and gas flow patterns

The effect of sparging gas bubbles into a stirred tank is to reduce substantially the power consumption of the impeller. In gas–liquid applications the

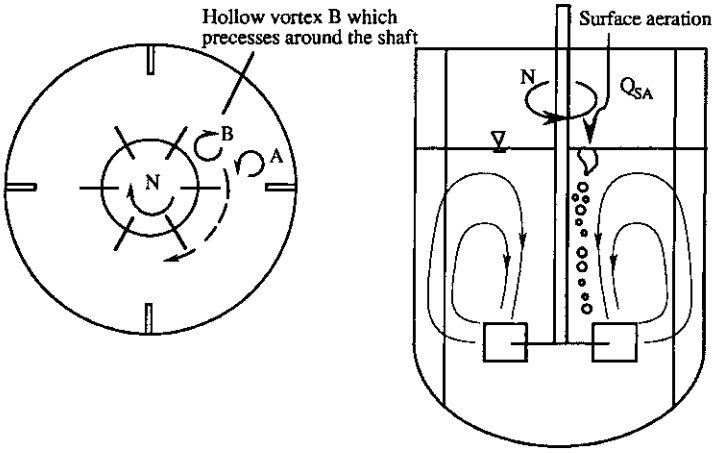

Fig. 10.15 Surface entrainment mechanism in baffled tanks.

gassed power input is fairly high (~1–2 kW m^{-3}) since large energy dissipation rates are required to produce small bubbles and large interfacial areas. Uhl and Gray (1966, Vol. I, pp. 145–148), Nagata (1975, Ch. 8) and Greaves and Barigou (1986) have reviewed the literature on power consumption under aerated conditions. The best-known correlation is by Michel and Miller (1962):

$$P_g = C\left(\frac{P_o^2 N D^3}{Q_g^{0.56}}\right)^{0.45} \tag{10.33}$$

where C is a constant with values between 0.63 and 1.19, depending on tank diameter and geometry (all units are in SI). Mann (1983) gives $C = 0.72$, but notes that equation (10.33) fails as the sparged gas volumetric flowrate $Q_g \to 0$ and as $Q_g \to \infty$; therefore caution should be exercised in using this method for scale-up.

More recently, workers have expressed their results in dimensionless terms by plotting the gassed power ratio P_g/P_o (taking values in the range 0–1) against the aeration number $N_A = Q_g/ND^3$, at constant impeller speed, as shown in Fig. 10.16. This figure is for a standard geometry disc turbine, but data are available in the literature for many other impeller designs. As the power input partly determines rates of mass transfer in gas–liquid dispersions, it is important that the gassed power number does not drop off too rapidly as the aeration number increases. The Rushton turbine was

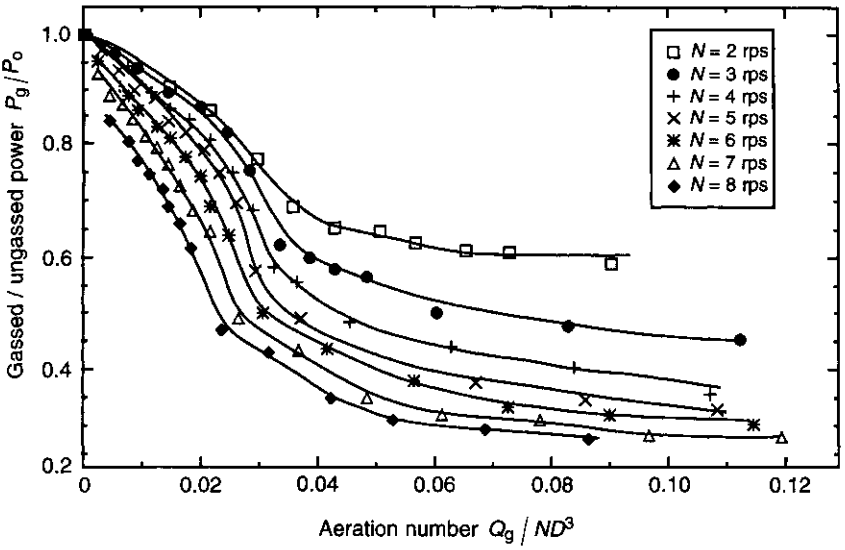

Fig. 10.16 Gassed power ratio for a standard disc turbine (van't Riet and Smith, 1973).

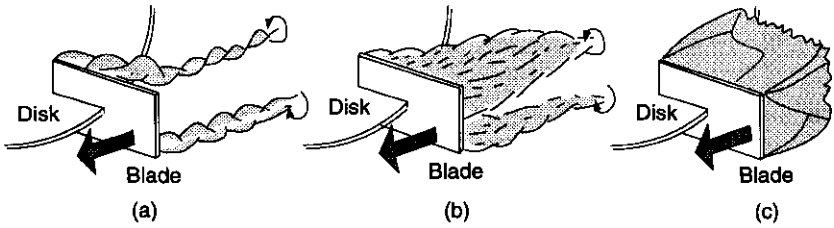

Fig. 10.17 Cavity shapes formed on blades during gas–liquid dispersion: (a) vortex cavities; (b) clinging cavities; (c) large cavities.

formerly regarded as an efficient gas disperser; however, it has a large ungassed power number, and the power decreases by as much as 60% on aeration. Modern developments in gas–liquid agitator design have concentrated on impellers that maintain a value of P_g/P_o close to 1 over the operating range of aeration numbers.

Bruijn *et al.* (1974) and van't Riet and Smith (1973) explained the decrease in gassed power consumption as a consequence of the formation of stable 'gas cavities' behind the blades. Gas sparged into the vessel is trapped in trailing vortices behind each impeller blade and may remain there for several revolutions before being dispersed as small bubbles in the highly turbulent wake of each cavity. For a continuous flow of gas, at a sufficiently high impeller speed, stable gas cavities form behind each blade; the size and shape of these cavities depends on gas volumetric flowrate and impeller speed, as illustrated by Fig. 10.17. At low gas flowrates the bubbles are trapped in the trailing vortex system behind each blade and form so-called **vortex cavities**. As the sparged gas flowrate is increased the attached cavity size increases, forming clinging and then large cavities. Smith and Warmoeskerken (1986) have published flow regime maps, of which Fig. 10.18 is an example, showing cavity types as a function of the Froude and the aeration numbers. For $N_A > \sim 0.06$ the cavities form themselves into a three–three configuration for six-bladed impellers: that is, there are large and small cavities on alternate blades. For five-bladed impellers the three–three configuration tries to form, but the large or small cavity precesses from blade to blade. The size of the attached cavity determines the drag coefficient for the blade, and thus the precessing cavity causes a fluctuating load on the blade and an imbalance of the forces acting on the shaft. It was quite common for the shafts of five-bladed impellers to break in gas–liquid operation, and their use is avoided today.

The presence of these cavities alters the liquid streamlines around the blade, so that the separation point occurs further downstream from the leading edge of the blade. Form drag on the impeller is decreased, as the wake volume behind each blade is reduced by the presence of the gas cavity. Consequently there is a reduction in power consumption in the presence of gas, which depends on the size and shape of the gas cavities.

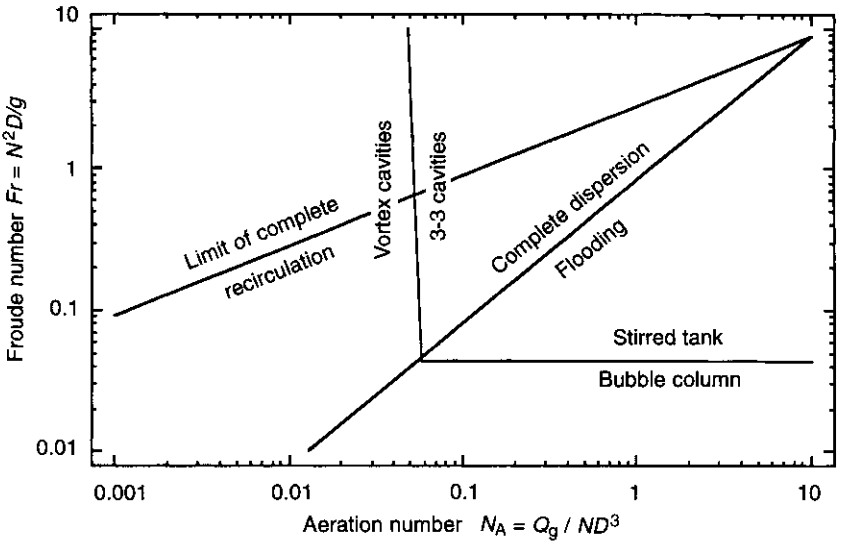

Fig. 10.18 Gas flow map for standard disc turbine, showing regions of different cavity formation.

Figure 10.19 demonstrates the effect on gas flow patterns in a gas–liquid stirred tank of gradually increasing the gas throughput or decreasing the impeller speed (Nienow *et al.*, 1978). At low gas flowrates and high impeller speeds the bubbles are well dispersed above and below the impeller; with increasing gas flow, the gas dispersion becomes worse. Nienow *et al.* (1978) defined a critical speed for complete dispersion, N_{CD}, at the change from conditions (c) to (d) in Fig. 10.19. For $H = T$, $C = T/4$, six-bladed disc turbines (valid for $T < 1.8$ m), Nienow *et al.* (1978) correlated their results by Pipe spargers:

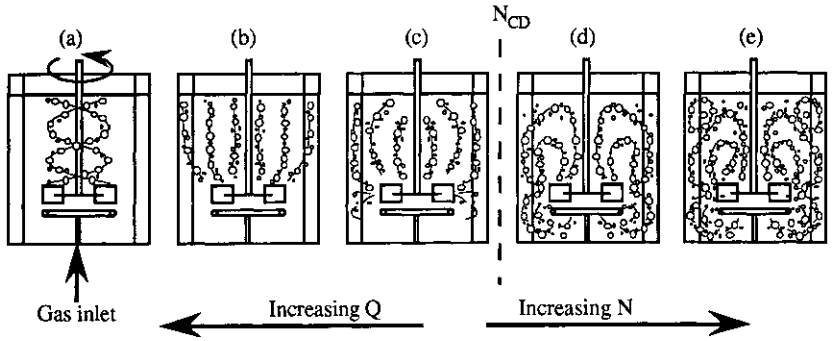

Fig. 10.19 Gas flow patterns as a function of impeller speed and gas flowrate.

$$N_{CD} = 4\frac{Q_g^{0.5}T^{0.25}}{D^2} \tag{10.34}$$

Ring spargers:

$$N_{CD} = 3\frac{Q_g^{0.5}T^{0.25}}{D^2} \tag{10.35}$$

Here Q_g is the volumetric flowrate of gas and all quantities are in SI units. These equations predict conservative values of N_{CD} for non-coalescing systems and turbines with more than six blades (Middleton, 1985).

Figure 10.16 shows that at constant impeller speed the gassed power ratio becomes fairly constant at large values of aeration number N_A. Under these conditions the cavities have grown to their maximum size; further increasing the gas throughput leads to 'flooding', corresponding to (a) in Fig. 10.19. In the flooded condition, not all the gas passes through the gas cavities and some is not dispersed by the impeller. At this point the impeller virtually stops pumping in the radial direction, and a bulk liquid circulation is set up by the rising bubbles (Warmoeskerken and Smith, 1984). These workers showed theoretically that at the flooding point

$$\frac{Q_g}{N_F D^3} = 1.2\frac{N_F^2 D}{g} \tag{10.36}$$

where N_F is the critical impeller speed for flooding at a given gas volumetric flowrate Q_g. Clearly, flooding is an undesirable condition, which should be avoided in practice as liquid-phase mixing, gas dispersion and gas–liquid mass transfer are all adversely affected.

In many gas–liquid operations the process objective is to maintain the same level of power input at different gas inputs: that is, to have a gassed power curve which is relatively flat, without much reduction in the ratio P_g/P_o. This ensures that bubble sizes and mass transfer coefficients are not impaired (see sections 10.5.3 and 10.5.4). Recent developments in impeller design have shown that large numbers of blades (12 or 18) or concave blades give this type of behaviour (Middleton, 1985).

10.5.3 Gas voidage fraction and interfacial area in stirred tanks

In designing gas–liquid reactors or fermenters it is necessary to know the gas volume fraction held up in the liquid, so that the overall volume of the vessel may be calculated. The mean gas voidage fraction ε is defined as

$$\varepsilon = \frac{V_G}{V_G + V_L} \tag{10.37}$$

where V_G and V_L are the gas and liquid volumes in the stirred tank, respectively. A large number of purely empirical correlations have been proposed

for the gas voidage fraction in terms of the gas flowrate and impeller speed. Calderbank (1958) presented a semi-theoretical method for predicting the mean gas voidage fraction; the method is based on Kolmogoroff's theory of local isotropic turbulence, which is valid only at high Reynolds numbers. The analysis shows that the **largest** bubble size that can exist in a given turbulent flow depends on the power input per unit volume, (P_g/V), the fluid density ρ_L and the surface tension σ:

$$d_{max} \propto \frac{\sigma^{0.6}}{\rho_L^{0.2}\left(P_g/V\right)^{0.4}} \tag{10.38}$$

Calderbank correlated the Sauter **mean** bubble diameter d_{32} (a surface area, volume mean) data from stirred-tank experiments using the expression

$$d_{32} = 4.15\left[\frac{\sigma^{0.6}}{\rho_L^{0.2}\left(P_g/V\right)^{0.4}}\right]\varepsilon^{1/2} + 9\times10^{-4}\ \text{m} \tag{10.39}$$

Using similar arguments Calderbank also proposed that the interfacial area per unit volume was given by

$$a = 1.44\left[\frac{\rho_L^{0.2}\left(P_g/V\right)^{0.4}}{\sigma^{0.6}}\right]\left(\frac{v_g}{V_\infty}\right)^{1/2} \tag{10.40}$$

where V_∞ is the terminal rise velocity of a single bubble and v_g is the superficial gas velocity. The interfacial area and gas voidage fraction are related by

$$d_{32} = \frac{6\varepsilon}{a} \tag{10.41}$$

for spherical bubbles, where d_{32} is a Sauter mean diameter. The important feature of equations (10.39) and (10.40) is that both the bubble size and specific interfacial area depend on the power input per unit volume. Clearly then the rate of mass transfer also depends on P_g/V, so that it is a requirement of any gas–liquid impeller that the gassed power is almost independent of the gas flowrate. Then the expression for the voidage fraction becomes (using equations (10.39)–(10.41))

$$\varepsilon = \left(\frac{v_g\varepsilon}{V_\infty}\right)^{1/2} + 2.16\times10^{-4}\left[\frac{\rho_L^{0.2}\left(P_g/V\right)^{0.4}}{\sigma^{0.6}}\right]\left(\frac{v_g}{V_\infty}\right)^{1/2} \tag{10.42}$$

Calderbank's method is only approximate, as it is well known that the power input to the tank is not dissipated uniformly (Laufhutte and Mersmann, 1985): more energy is dissipated in the vicinity of the impeller

than in the bulk circulation. Consequently there is a distribution of bubble sizes and voidage fractions throughout the vessel. A further drawback to these equations is that the **gassed** power consumption is required; section 10.5.2 has already shown that this is not a straightforward quantity to calculate.

An alternative to Calderbank's method is to use a purely empirical correlation that covers a wide range of variables. Smith *et al.* (1977) proposed that for

Coalescing systems:

$$\varepsilon = 0.02\left(\frac{P_g}{V_L}\right)^{0.475}\left(v_s\right)^{0.4} \tag{10.43a}$$

for

$$0.005 \leqslant v_s \leqslant 0.05\,\mathrm{m\,s^{-1}}$$

and

$$1 \leqslant \left(\frac{P_g}{V_L}\right) \leqslant 5\,\mathrm{kW\,m^{-3}}$$

Non-coalescing systems:

$$\varepsilon = 0.04\left(\frac{P_g}{V_L}\right)^{0.475}\left(v_s\right)^{0.4} \tag{10.43b}$$

for

$$0.004 \leqslant v_s \leqslant 0.02\,\mathrm{m\,s^{-1}}$$

and

$$100 \leqslant \left(\frac{P_g}{V_L}\right) \leqslant 750\,\mathrm{W\,m^{-3}}$$

All quantities are in SI units. The results were obtained on tanks up to 1.8 m diameter, but equations (10.43a) and (10.43b) do however contain dimensional constants, which may change on scale-up.

10.5.4 Gas–liquid mass transfer

Many mixing problems involve the transfer of a solute gas into the liquid phase for subsequent chemical reaction (as in aerobic fermentations, for example). This process has been introduced in section 4.9.1. The process objectives of these operations are to disperse the sparged gas as small bubbles (and therefore create gas–liquid interfacial area) and to generate turbulence to increase mass transfer rates. Large interfacial areas require

small bubble sizes and large gas voidage fractions (see equation (10.41)). The general equation for mass transfer between a liquid and a gas (where chemical reaction kinetics are not rate determining) is

$$J = K_L a\left(c_L^* - c_L\right)V \tag{10.44}$$

where J is the molar transfer rate of species A per unit volume; K_L is the overall liquid phase mass transfer coefficient; a is the interfacial area per unit volume; c_L is the liquid-phase molar composition; c_L^* is the equilibrium liquid-phase molar composition; and V is the volume of the dispersion. In some cases the liquid-phase resistance predominates, and the overall mass transfer coefficient K_L is equal to the liquid film coefficient k_L (see Kay and Nedderman, 1985, Ch. 18). Experimental techniques do not usually allow separate determination of k_L and a, and so most workers have measured the product $k_L a$. For example, in air–water and air–electrolyte solutions (Smith *et al.*, 1977):

Coalescing systems:

$$k_L a = 0.01\left(\frac{P_g}{V_L}\right)^{0.475}\left(v_g\right)^{0.4} \tag{10.45a}$$

Non-coalescing systems:

$$k_L a = 0.02\left(\frac{P_g}{V_L}\right)^{0.475}\left(v_g\right)^{0.4} \tag{10.45b}$$

where v_g is the gas superficial velocity ($v_g = 4Q_g/\pi T^2$).

The units are SI and the ranges of applicability are the same as for equations (10.43a) and (10.43b). Note that addition of surface active agents (such as anti-foam) significantly affects the value of the interfacial area per unit volume and therefore has a large effect on mass transfer.

Measurements of mass transfer rates in agitated vessels are not easy to make and considerable controversy surrounds the interpretation of data from oxygen or carbon dioxide absorption tests or from chemical absorption tests. That, together with obtaining data on real fermentation systems, makes the design of gas–liquid reactors a difficult art.

10.6 Liquid–liquid dispersions and the creation of emulsions

The two properties of liquid–liquid mixtures or emulsions that are of particular relevance to the food industry are rheology and stability. In liquid–liquid extractions, the formation of a droplet dispersion is an intermediate processing step in which stability is only required over a sufficiently long period to allow phase equilibrium to be established. Subsequent processing requires that the mixture be separated by coalescence of the droplets and so

long-term stability would actually hinder the process. A second category of liquid–liquid processes is the manufacture of stable emulsions (for example, the manufacture of margarines and spreads): emulsion rheology gives consistency and texture to the product, while stability ensures that the material does not separate during a long shelf-life. Both these properties are related to droplet size, dispersed phase volume, interfacial tension, and attractive/repulsive forces between droplets. During production of emulsions, surface-active ingredients (emulsifiers) are often added to reduce interfacial tension and to prevent coalescence of droplets.

Stresses in the fluid due to motion of the impeller cause primary drops to elongate and finally break up into droplets and much smaller satellite droplets. These events occur many times, until an equilibrium is established between the rates of break-up and coalescence. Thus during a batch-mixing operation the mean droplet size decreases to a steady value, and thereafter remains approximately constant. Theoretical methods exist to predict the break-up of droplets in idealized flow conditions, but not in realistic mixer geometries: the dynamics of droplet break-up are complex and are outside the scope of this chapter [refer to Donaldson (1985) for introductory material]. Many emulsifications take place under turbulent flow conditions; approximate models based on Kolmogoroff's theory of local isotropic turbulence yield that the maximum droplet diameter depends on the surface tension σ, continuous phase density ρ_c and the specific power input per unit volume (P/V), in an analogous way to the break-up of gas bubbles (see section 10.5.3):

$$d_{\max} \propto \frac{\sigma^{0.6}}{\rho_c^{0.2}\left(P/V\right)^{0.4}} \tag{10.46}$$

where the constant of proportionality depends on the tank and impeller geometry. Alternatively, this may be written in terms of a critical **Weber number** for the maximum droplet size We_c:

$$We_c = 2.0\frac{\rho_c^{1/3} d_{\max}^{5/3}\left(P/V\right)^{2/3}}{\sigma} \tag{10.47}$$

Again, the value of the critical Weber number depends on tank and impeller geometry. The local specific power input in the vicinity of the impeller (where fluid stresses are largest and droplet break-up occurs) may be many times the average value of P/V. McManamey (1979) assumed that the power input was dissipated in the volume swept out by the impeller and correlated a variety of data for the Sauter mean diameter d_{32} from different impeller systems by

$$d_{32} = C_1\left[\frac{4}{\pi}N_{po}\frac{D}{W}\right]^{-0.4} We^{-0.6} \tag{10.48}$$

where

$$We = \textbf{impeller}\ \text{Weber number} = \frac{\rho_c N^2 D^3}{\sigma} \tag{10.49}$$

Here the constant C_1 has a value of 0.22 ± 20%, independent of impeller type. Equation (10.48) applies to systems with a low volume fraction of dispersed phase, where coalescence does not occur as droplets move away from the impeller region. Lee *et al.* (1984) examined the effect of phase volume fraction ϕ on the Sauter mean drop size in stabilized systems, and proposed a correlation of the form

$$\frac{d_{32}}{D} = k_1\left(1 + k_2\phi\right)We^{-0.6} \tag{10.50}$$

where *We* is given by equation (10.49), and the constants k_1 and k_2 depend on agitator design and the liquid–liquid system.

10.7 Solids suspension and solid–liquid mass transfer

In solid–liquid stirred-tank applications the process objectives fall into the following categories:

- suspension of particles initially resting on the bottom of the tank, so as to expose the maximum solid–liquid surface area for mass transfer;
- formation and maintenance of a homogeneous suspension of particles (this is a particular requirement of continuous systems with draw-off of liquid–solid mixture);
- suspension of particles in order to obtain flocculation (this requires gentle agitation to suspend the solids and promote collisions between particles, but without excessive shear, which breaks weak flocs).

Typical solid–liquid operations are dissolution (formation of sucrose syrups, for example), fermentations (suspension of cell cultures and growth media, for example), crystallization, and continuous slurry draw-offs from stirred tanks, used as premixers or holding vessels. In the latter case the objective is to keep the solids in suspension, avoiding sedimentation and segregation. Drawing off product from a mixture that is not fully suspended or has axial concentration gradients would give varying solids fractions as the vessel was emptied.

The usual criterion for **complete suspension** is that 'no particle should remain on the bottom of the tank for more than 1–2 s' (Zwietering, 1958). Measurements of the 'just suspended' impeller speed N_{JS} or impeller power P_{JS} are obtained by gradually increasing and decreasing the impeller speed in a transparent tank until the criterion is satisfied. Although this is a subjective measurement, the results are fairly reproducible because the last particles to be suspended are usually trapped in the relatively stagnant

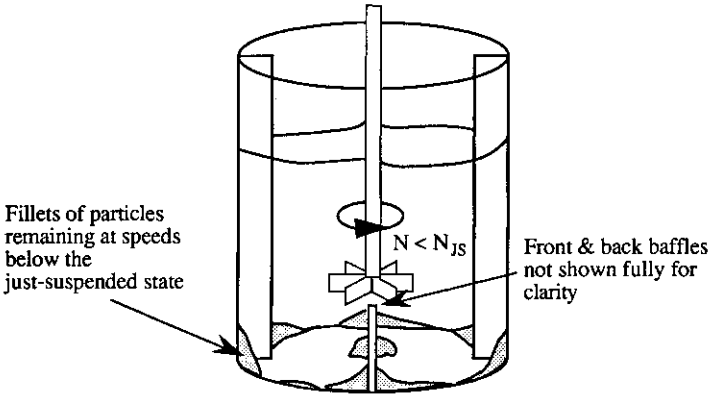

Fig. 10.20 Stagnant regions near corners and baffles, where fillets of solids collect. These are usually the last particles to be suspended.

zones located directly beneath the impeller or behind the baffles on the base of the tank (see Fig. 10.20).

A less rigorous definition of the just-suspended condition allows a small fraction of particles to remain as fillets in these stagnant regions (Fig. 10.20) but no other particles rest on the tank bottom for more than 1–2 s. This type of suspension results in considerable savings in power input (and hence agitator and shaft size) compared with satisfying Zwietering's criterion, which generally requires intense agitation (~1–2 kW m^{-3}; Nienow, 1985). If only a small fraction of particles remain motionless, then the solid–liquid mass transfer area is only slightly reduced.

Homogeneous suspension requires that no solids concentration gradients are present within the vessel: that is, the solids are uniformly distributed. The impeller speed to obtain homogeneous suspension is considerably higher than for complete suspension and operation under these conditions is not usually economically feasible. The homogeneous condition is difficult to determine experimentally; a common technique is to sample the mixture at various heights in the vessel. However, it is difficult to ensure representative, isokinetic sampling: in most regions of the tank there is relative motion between the particles and the liquid and therefore the sample withdrawal velocity cannot be made equal to the velocity of the flowing mixture.

For the case where samples can be obtained isokinetically from all parts of the tank, the homogeneous condition may be defined in terms of a mixing index M:

$$M = \frac{\sigma}{\bar{x}} = \frac{\sqrt{\sum_{i=1}^{n} \frac{\left(x_i - \bar{x}\right)^2}{\left(n-1\right)}}}{\bar{x}} \tag{10.51}$$

where x_i is the solids concentration of sample i (kg solids/kg mix); σ^2 is the variance of solids concentration (kg/kg)^2; n = number of samples; and

$$\bar{x} = \text{mean solids concentration in tank} = \sum_{i=1}^{n} \frac{x_i}{n} \qquad \left(\text{kg/kg}\right) \quad (10.52)$$

For a perfectly homogeneous tank the mixing index would be zero; typically, the tank could be said to be homogeneous when $M \leqslant 0.05$. This method requires a large number of samples to be withdrawn from the tank during operation and analysed, for example, by separating the liquid and solid phases, and drying.

Many authors have measured the impeller speed to obtain the 'just suspended' state. Zwietering's (1958) correlation covers the widest range of fluid properties, particle size, concentration and properties, and tank geometric parameters:

$$N_{JS} = s\nu_L^{0.1} d_p^{0.2} \left(\frac{g\Delta\rho}{\rho_L}\right)^{0.45} D^{-0.85} x^{0.13} \quad (10.53)$$

The dimensionless constant s in equation (10.53) depends on impeller type, clearance ratio T/C, and diameter ratio T/D. Zwietering (1958) and Nienow (1968) presented graphs of s versus T/D at various T/C for propellers, disc turbines, vaned discs and flat blades. These data may be correlated using expressions of the form

$$s = a\left(\frac{T}{D}\right)^b \quad (10.54)$$

where a and b are constants that depend on T/C and impeller type.

The correlation in equation (10.53) is dimensionless and is generally accepted as giving a conservative estimate for N_{JS}. Nienow (1968) confirmed the exponents and constants in Zwietering's correlation using data obtained in an independent study.

For dissolution of solid particles (without chemical reaction) the rate of mass transfer (kmol s^{-1}) is given by

$$J = k_s A\left(c_s - c_\infty\right) \quad (10.55)$$

where A is the exposed solid–liquid contact area and k_s is the mass transfer coefficient. Note that equation (10.55) applies to operations in which diffusion controls mass transfer from the particles to the bulk fluid at concentration c_∞; c_s is the saturation concentration at the surface of the particles. The dissolution of solid particles should be carried out at an impeller speed in excess of N_{JS}, such that the maximum liquid–solid surface area is exposed. Operation at high impeller speeds ($N > N_{SA}$) leads to entrainment of air from the free surface, which blankets the particle surfaces, and mass transfer rates remain approximately constant, independent of speed.

Nienow and Miles (1978) showed that the diffusion-controlled mass transfer coefficient k_{JS} at the just-suspended speed N_{JS} was independent of the impeller and tank configuration (that is, k_{JS} does not depend on the specific power input P/V). In this case the impeller and tank configuration should be chosen to be the most economic in terms of power consumption and the impeller speed should be in the range $N_{JS} < N < N_{SA}$. In this range of speeds, the mass transfer coefficient varies as

$$k_s \propto N^a \qquad \text{where } a = 0.4\text{–}0.6 \tag{10.56}$$

To achieve the just-suspended condition often requires large specific power inputs: increasing the impeller speed leads to small increases in the mass transfer coefficient (equation (10.56)), but large increases in power demand ($P \propto N^3$). Thus operating much above the just-suspended condition may be uneconomic (Nienow, 1985).

The mass transfer coefficient may be predicted from a correlation similar to the Froessling equation for particle–fluid systems [Rowe *et al.*, 1965 and equation (4.23)]:

$$Sh = 2 + 0.72 Re_p^{1/2} Sc^{1/3} \tag{10.57}$$

The Schmidt number is

$$Sc = \frac{\mu_L}{\rho_L \mathcal{D}} \tag{10.26}$$

and the Sherwood number is

$$Sh = \frac{k_s d_{32}}{\mathcal{D}} \tag{10.58}$$

In equation (10.57) d_{32} is the mean particle diameter, $\mathcal{D}$ is the liquid phase diffusion coefficient and the particle Reynolds number is

$$Re_p = \frac{\rho_L d_{32} v_s}{\mu_L} \tag{10.59}$$

where v_s is the slip velocity between the particle and liquid. Clearly, this velocity is not well defined in a complex flow such as in a stirred tank, and is difficult to calculate. One approach is based on Kolmogoroff's theory of isotropic turbulence, which shows that the Reynolds number may be written as

$$Re_p = \frac{\varepsilon_T d_{32}^4}{\nu_L^3}$$

where

$$\varepsilon_T = P/\rho_L V = \textit{average} \text{ specific power input } \left(\mathrm{W\,kg^{-1}}\right)$$

$$\nu_L = \mu_L/\rho_L$$

A second approach described by Nienow (1985) is based on the slip velocity being approximately equal to the particle terminal velocity, but both methods have their drawbacks. Calculation of the mass transfer coefficient may be carried out using equations (10.57)–(10.60). The liquid–solid mass transfer area per unit volume is unknown and must be calculated from the Sauter mean particle size d_{32} and the volume fraction of particles in suspension, α:

$$a = \frac{6\alpha}{d_{32}} \tag{10.61}$$

The overall mass transfer rate can now be calculated from equation (10.55), knowing the concentrations of solute material in the bulk flow and at the surface of the particle.

10.8 Scale-up of mixers from pilot trials

In many situations there is no clear-cut design method available and the only remedy is to make measurements on a pilot-scale mixer and scale up to plant-scale operation. This is not a straightforward exercise, particularly when more than one parallel or series unit operation occurs within the mixer. In the previous sections a number of design equations have been presented that should allow the engineer to make **estimates** of the speed, power and tank configuration to achieve the desired process result. Wherever possible, these equations have been given in dimensionless form: that is, they make use of the principal of similarity to ensure that geometric, dynamic or kinematic conditions remain the same, regardless of the scale of operation (Ch. 2).

Similarity	*Quantities remaining constant*
geometric	all geometric ratios
kinematic	velocities at geometrically similar points
dynamic	ratios of forces, e.g. equal *Re*, *Fr* or *We*

These methods allow extrapolation of results obtained on a small-scale experiment to full scale, assuming that all pertinent variables have been included in the original dimensional analysis and that the systems are fluid-dynamically similar. Design equations that contain dimensional constants should always be treated with caution; it would be unwise to extrapolate results much outside the range of the original experimental data.

There are several problems associated with maintaining similarity at different scale, as follows.

- In many operations (such as solids suspension, or gas–liquid mass transfer) the size of the particles or bubbles remains approximately constant while the dimensions of the mixer increase significantly.

- Physical constraints may preclude maintaining geometric similarity. For example, in fermenter design the ratio of reactor surface area to volume decreases with increasing scale. This means that it becomes increasingly difficult to remove the heat of reaction from the fermenter if geometric ratios remain constant. Typically, the aspect ratio of the reactor is increased at larger scales.
- The scale of scrutiny for the mixture should remain the same regardless of scale, as it is determined by the end use of the product. Therefore the range of length scales from the unmixed to mixed states may be greater at larger scales.
- Pilot-scale experiments can never be designed to cover all possible variables that might affect the process result. Therefore any model derived is likely to be incomplete in all details and some contingency should always be allowed during scale-up.
- Ensuring dynamic **and** kinematic similarity can give conflicting results. Scale-up using kinematic similarity may result in a change of flow regime, as the Reynolds number increases with increasing scale and therefore a different form of correlation might apply.

Two common scale-up rules have been widely applied in the past:
Constant power per unit volume

$$\frac{P_1}{V_1} = \frac{P_2}{V_2} \tag{10.62}$$

Constant tip speed

$$N_1 D_1 = N_2 D_2 \tag{10.63}$$

In the turbulent regime the power per unit volume varies as (see equations (10.5) and (10.13))

$$\frac{P}{V} \propto \frac{N^3 D^5}{T^3} \propto N^3 D^2 \tag{10.64}$$

so that at **constant tip speed**, equations (10.63) and (10.64) show that

$$\frac{P}{V} \propto \frac{1}{D} \tag{10.65}$$

That is, as the scale increases the specific power input decreases. Clearly then, the first rule gives a more conservative estimate of full-scale operating conditions (except for systems that might be damaged by overmixing or for liquid blending). The constant power per unit volume rule may, however, lead to a grossly oversized and uneconomic design. Table 10.4 illustrates some of the difficulties in maintaining similarity. In Table 10.4 all parameters at the pilot scale are assigned a value of 1, enabling comparison of their relative changes on scale-up. In each of the last three columns the

Table 10.4 The effect of scale-up by a factor of 5 on mixer properties (geometrically similar systems)

Property	Pilot Scale	Plant Scale		
		Constant P/V	Constant πND	Constant Re
Impeller diameter, D	1.0	5.0	5.0	5.0
Power, P	1.0	125	25	0.2
P/V	1.0	[1.0]	0.2	0.0016
Speed, N	1.0	0.34	0.2	0.04
Pumping capacity, Q_L	1.0	42.5	25	5.0
Tip speed, πND	1.0	1.7	[1.0]	0.2
Reynolds Number, $\frac{\rho_L ND^2}{\mu_L}$	1.0	8.5	5.0	[1.0]

power input per unit volume, tip speed and Reynolds number are held constant, respectively. Note that for turbulent flow, dimensionless numbers such as N_{po}, $N\theta$, N_Q are independent of Reynolds number and so dynamic similarity of Re can be relaxed. Clearly choosing one scale-up rule rather than another has a very large impact on the full-scale design, even when the scale factor is only 5.

Some operations, such as solids suspension, are notoriously difficult to scale up, and there are many conflicting rules presented in the literature: for example Voit and Mersmann (1986) report that the scale-up rule for solids suspension is $P/V \propto D^a$, where the literature values of a vary between –0.7 and +0.5! These problems are further compounded in three-phase reactors, where gas–liquid dispersion, liquid-phase mixing and solids suspension may all be required simultaneously: gas–liquid dispersion is often scaled using constant power input per unit volume, liquid blending may be scaled using equal impeller speeds ($N\theta$ = constant) for equal blend times, and there is no clear-cut method for the last operation. Usually the power requirement for scaling liquid blending on equal impeller speed is not feasible and longer blend times are used at larger scales.

It should be clear from this discussion that a great deal of art remains in overcoming the scale-up problem and that successful design depends as much on experience as on fundamental science.

10.9 Alternative mixing devices

The discussion in the previous sections of this chapter has concentrated on the design of stirred-tank mixers for low- and high-viscosity fluids. The range of mixing problems encountered in the food and chemical process industries is vast, and often more specialized mixing devices are required.

For very high-viscosity materials (such as bread or biscuit doughs, which cannot be handled by anchor or helical ribbons), **kneaders** or **Z-blade mixers** are used (see Fig. 10.21). Generally, these mixers are mounted horizontally and have two counter-rotating blades; clearances between the blades and trough are very close so as to eliminate stagnant regions and eliminate build-up of sticky material on the wall. Mixing is achieved by a combination of bulk movement and intense shearing and extensional flow as the material passes between two blades or between the wall and a blade.

Some comminution processes (such as the dispersion of fine powders or emulsifications) cannot be carried out in conventional stirred tanks because it is not possible to generate large enough shear stresses to break down agglomerates or particles. In these cases, ball mills or dispersion mills may

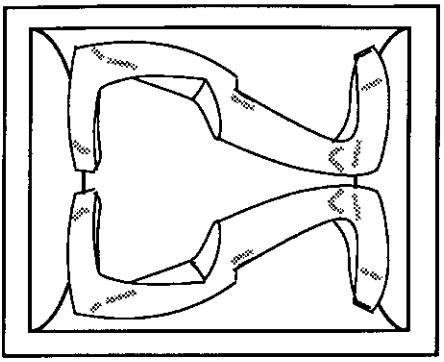

Fig. 10.21 Schematic diagram of a Z-blade mixer.

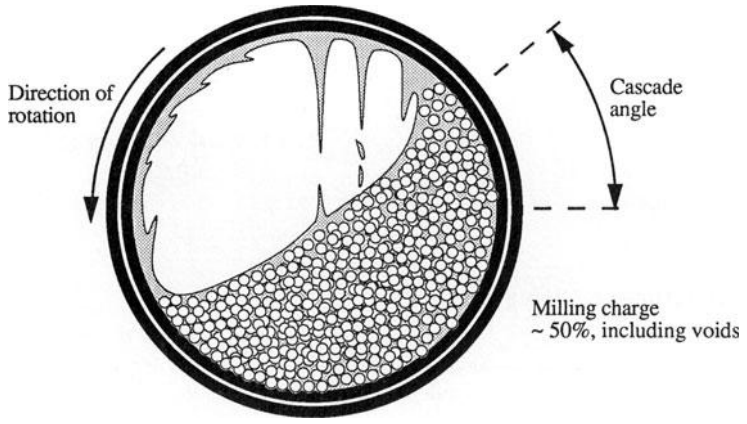

Fig. 10.22 The ball mill.

be used to break aggregates or to form stable emulsions. The **ball mill** (Fig. 10.22) consists of a horizontally mounted, cylindrical drum, which is partially filled with high-density metal balls. The outer drum rotates slowly allowing the balls to roll over each other by gravity, creating very large shearing forces in the 'nip' between adjacent balls. The ball mill generally operates about half-full of balls, at a rotational speed that is about 60% of that for the balls to be thrown out to the walls by centrifugal force. This gives a cascade angle of about 20–30°. These devices are difficult to use in the food industry as the balls wear and may, in severe conditions, chip or shatter.

Dispersion mills (Fig. 10.23) make use of a very high-speed rotor blade, which moves inside a slotted stator. Close clearances between the rotor and stator give high shear stresses, which may be used for droplet or aggregate break-up, while the flow through the slots drives gross circulations within the vessel. These devices are suitable for the formation of emulsions: droplet break-up takes place in the high-energy dissipation regions close to the disperser head. The droplets are dispersed in the bulk liquid by the convective flow issuing from the head.

Screw extruders (Fig. 10.24) are often used in polymer processing and also have some applications in the food industry: for example, in the manufacture of reconstituted potato or corn snacks. Raw ingredients are added through a feed hopper and are conveyed by a rotating horizontal screw. High pressures and temperatures are generated within the barrel of the extruder, such that the food material is rapidly cooked, before being extruded through a die. Single or double counter-rotating screws are used, although the latter give more intense mixing at the expense of greater

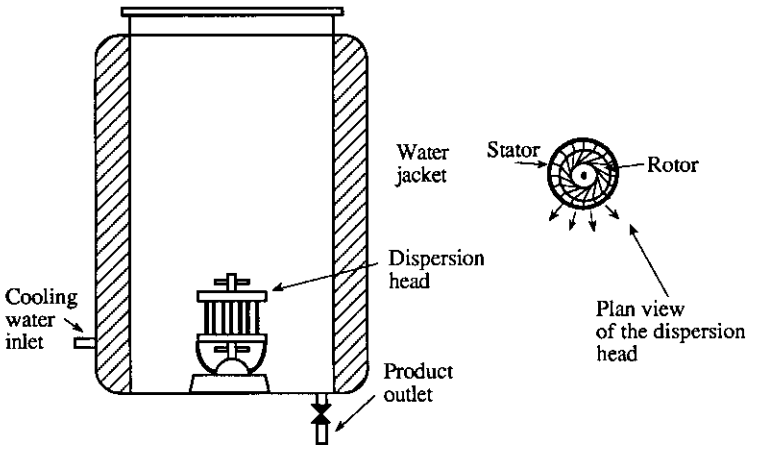

Fig. 10.23 Schematic diagram of a dispersion mill.

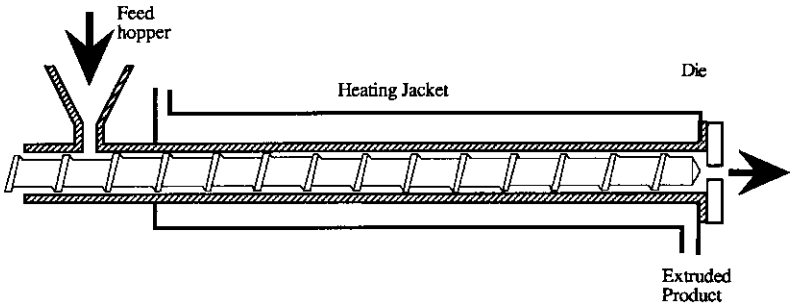

Fig. 10.24 Schematic diagram of a single-screw extruder.

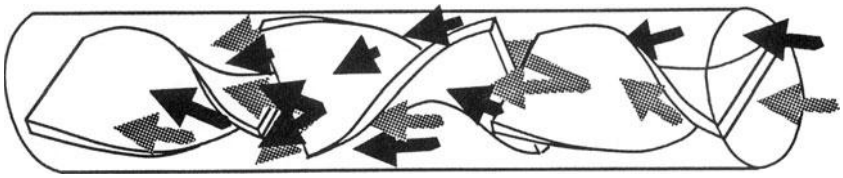

Fig. 10.25 Schematic diagram of an in-line mixer.

capital and running costs. The performance of single-screw machines can be improved by adding extra mixing heads or by using in-line static mixers.

The final category described in this section is **in-line static mixers**, so called because they have no moving parts and do not require a mechanical drive. The mixer consists of a number of mixer elements inserted in a length of straight pipe (Fig. 10.25). Mixing is achieved using the energy available in the liquid and results in a pressure loss as the process fluid passes through the mixing elements. The usual arrangement is to pump the raw ingredients through a length of pipe containing a number of static mixer elements (Fig. 10.25): the more difficult the mixing operations, the more elements are required. In the laminar regime, each static mixer element performs a cutting and twisting operation, as shown schematically in Fig. 10.5, so that after passing through a number of elements the scale of segregation (or the striation thickness) has been reduced to an acceptable level. The number of mixer elements, M, required in any application to reduce the striation thickness from δ_o to a smaller value δ is given by an expression of the form (Streiff, 1979)

$$\frac{\delta_o}{\delta} = \frac{1}{2^M} \tag{10.66}$$

for the mixer of Fig. 10.25, which offers *two* possible flow paths at each element.

Clearly then, static mixers are efficient for laminar blending operations, as doubling their volume squares the amount of mixing that occurs (as measured by a decrease in striation thickness).

Under turbulent flow conditions, the elements generate high turbulence intensities and promote rapid heat and mass transfer. The energy for mixing is provided by sizing the pump to give a larger pressure differential than would be required to overcome friction in an empty pipeline. Wilkinson and Cliff (1977) investigated the laminar flow pressure drop in a Kenics static mixer and proposed a modified form of the pipe flow pressure drop equation (see Ch. 2):

$$\Delta p = K \frac{4C_f \rho v^2 L}{2D} \tag{10.67}$$

where v is the velocity in the empty pipe, L is the length of the mixer and D is the internal diameter of the empty pipe. The factor K is the modification factor, which depends on Reynolds number and type of mixer elements.

These mixers are used for blending viscous materials [often with very different fluid properties, see Streiff (1979)], liquid–liquid droplet dispersion and incorporation of powders into liquids to form pastes. The essential difference between these devices and the mixers discussed previously is that in-line static mixers are intended to operate in continuous processes. Although the mixing within the elements is intense, the quality of the product depends on the operator's ability to ensure that the raw ingredients are supplied at the correct flowrates and in the right proportions. Therefore, if metering of the ingredients to the mixer is poor, the product will be homogeneous but may not match the required specification.

The design of static mixers (the number and type of mixing elements, and the pressure drop) have been much studied in the open literature, and much commercial information is available from mixer vendors (for example, Sulzer or Chemineer Kenics). A detailed description of the various types of in-line mixer is outside the scope of this chapter.

10.10 Mixing of particulate materials

In contrast to the fluid-mixing operations previously discussed, the mixing of solids is not an irreversible process. Mixtures of particles have a tendency to segregate or unmix owing mainly to differences in size between components; differences in density, shape, roughness and coefficient of restitution can also have a minor effect on segregation. Segregation occurs mainly because of the percolation of fine particles within the mixture: fines fall into gaps between large particles, slowly percolating to the bottom of the mixture, while large particles tend to rise to the top. Percolation segregation is

surprisingly effective even when there are only small differences (~20%) in particles size. Examples of this situation are:

- **Vibration of a solid mixture.** This is the mechanism that results in the nuts and raisins (large particles) moving to the top of a pack of muesli, during transit.
- **Shearing of a solid mixture.** One layer of particles moves at a different velocity from another layer: small particles tend to percolate into the lower layer.
- **During pouring or discharge from a vessel or hopper into a heap.** Large particles roll down the surface of the heap, while smaller particles percolate through the surface layer into the stationary bulk. This method is used to separate coarser table sugar from caster sugar, using the difference in particle size.

Segregation can also occur because of differences in particle trajectories, during free fall or horizontal motion. These effects are a result of the particles having different drag coefficients (which depend on the particle Reynolds number) and different inertia.

The other significant difference between solids and fluid mixing is that there is no equivalent molecular diffusion effect in powder mixtures. In fluid mixtures this mechanism brings about complete homogenization, if given sufficient time and is particularly important in the final stages of mixing. In solids mixing, however, motion of the particles can only be achieved by input of energy to the system, and the final equilibrium state is determined by the mixer design and the particle-segregating properties.

10.10.1 The nature of particulate materials

Granular materials may be broadly grouped into two categories: (a) **free-flowing** or **cohesionless powders** and (b) **cohesive powders**. These characteristics may be easily identified by observing the discharge of a granular material from a hopper. The free-flowing material discharges smoothly, at a constant flowrate, whereas the cohesive powder discharges intermittently or not at all because of bridging within the hopper. Cohesion within a material is caused by interparticulate bonding forces due to moisture (formation of liquid bridges between particles or the overlap of adsorbed moisture layers on the surfaces of adjacent particles), electrostatic attractions, and van der Waals forces. The latter are only significant for particles less than about 1 μm diameter. In general, these bonding forces become less significant as the particle size increases. As a rough rule of thumb, particles with sizes greater than about 100 μm behave as free-flowing powders and are likely to segregate if components with different sizes are present. Particles with sizes less than 10 μm behave as cohesional mixtures and do not segregate easily, but may form agglomerates or aggregates. Geldart (1973)

has presented a more detailed method of classifying powders according to their fluidization behaviour.

10.10.2 Solids mixers

There is a wide variety of solids mixers available. Harnby (1985) categorizes these mixers according to their mixing action.

Tumbler mixers. The particulates to be mixed are charged into a full enclosed vessel (typical designs are the roto-cube, double cone, Y- or V-shaped mixer: see Fig. 10.26). The vessel is filled to about half its total capacity and is rotated on an axis between two bearings, causing the solid particles to roll or tumble over each other continuously. The rotational speed is about half the critical speed at which centrifugal forces throw the solids out to the extremities of the container, and there is no relative motion of the particles. At the completion of mixing, the vessel may be removed from the mixer stand and transported to the next stage of the batch process.

Convective mixers. The solids are mixed in a stationary vessel by a rotating impeller or screw, which convects particles within the mixture. Examples of this type are:

- the **ribbon blender**, in which a helical blade (or Z blade) sweeps through a horizontal open trough or closed cylindrical vessel (Fig. 10.27). The

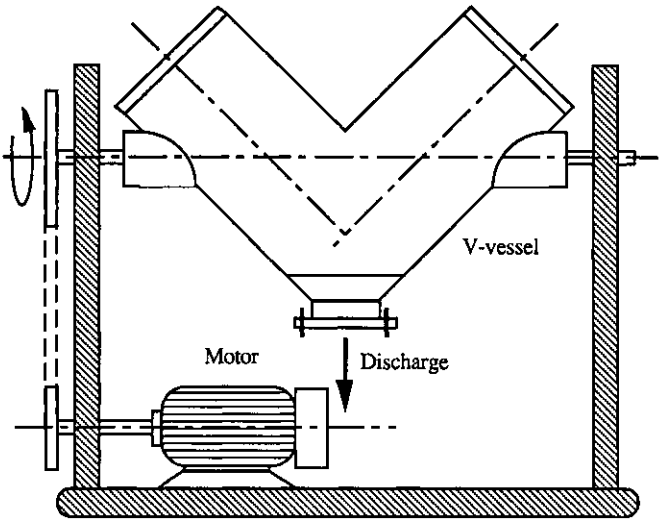

Fig. 10.26 V-shaped tumbler for solid–solid mixing.

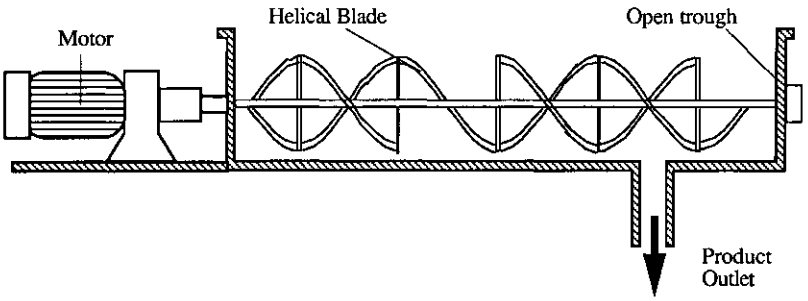

Fig. 10.27 Schematic diagram of a ribbon blender in an open trough.

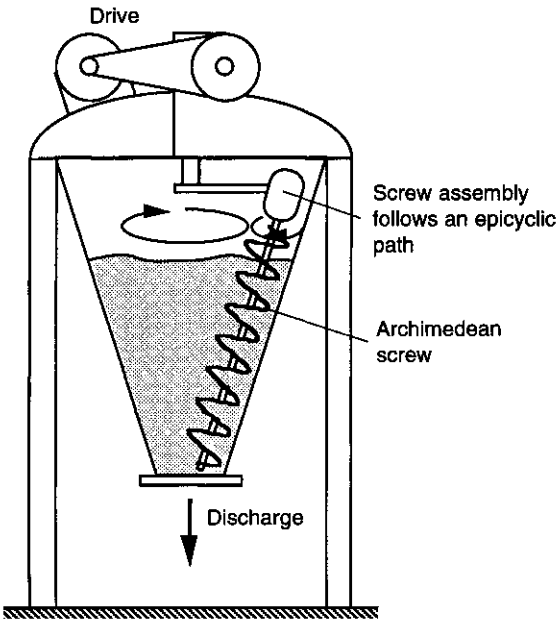

Fig. 10.28 The Nautamix convective mixer for solid–solid mixing.

mixer speed is generally low (<60 rpm) to minimize power input, heating of the mixture and particle degradation.

- the **Nautamix**, in which a small-diameter Archimedean screw rotates within a vertical, conical hopper (Fig. 10.28). Only particles in the vicinity of the screw are convected, but the driving action describes an epicyclic path within the hopper so that the blade progressively sweeps through all parts of the mixture.

Table 10.5 Selection of powder mixers

	Tumbler mixers	Convective mixers	Recirculating hoppers
Cleaning/sterility	Fully enclosed batch vessel, which may be constructed with smooth corners and with a polished surface finish or any other lining. No contact of the powder mixture with bearings or any other moving parts.	Bearings are in contact with the solids and there is a potential lubricant contamination problem. Vessels can have corners that are difficult to clean. Open troughs or vessels can disperse fine particles into the atmosphere: a dust hazard.	Difficult to flush out complete system between batches or if product specification changes frequently.
Particle degradation	Gentle action and low power input does not give comminution. Can only be used to mix weakly cohesive mixtures.	Low speed: little comminution. High speed: may be used to break down granules or agglomerates. Suitable for cohesive mixtures.	Negligible if recycle is by pneumatic conveying. Not suitable for strongly cohesive powders.
Controlled additions and heat transfer	Difficult to add materials during the mix without stopping the mixer. Addition of moisture creates large agglomerates, which are not easily broken. Difficult to use a cooling jacket.	Easily achieved, particularly with open troughs or vessels. Vessels may be jacketed to remove heat generated during mixing.	Easily achieved.
Batch or continuous operation	Not easily adapted for continuous use.	Possible to use as a batch or continuous mixer, although sufficient residence time must be allowed in the mixer to give the required degree of back-mixing. The amount of back-mixing depends on the impeller design.	Possible to use as a batch or continuous mixer.
Segregation	Rolling or tumbling motion promotes segregation and gives poor mixture quality (Harnby, 1967).	Large-scale circulation patterns reduce the amount of segregation. Good mixture quality achieved for strongly segregating materials (Harnby, 1967).	Segregation may occur due to percolation of small particles as the recycle flow pours onto a heap at the top of the hopper, or due to shear within the bulk flow.

Hopper mixers. During the discharge of a granular material from a hopper there are significant relative motions of the particles because of velocity gradients near the outlet orifice. Radial and axial mixing of different particulate components may be achieved by recycling the discharged material to the top of the hopper. This method relies on the powders being free-flowing and can be improved by collecting the discharge from several outlet locations within the hopper and combining them for recycling.

Table 10.5 summarizes the features of these mixer types and their suitability for various food-mixing operations.

Conclusions

There is surely no need to stress the importance of mixing operations, and their importance, for food processing. This chapter has introduced some of the key engineering aspects of such operations, covering the mixing of homogeneous liquids, liquid/liquid systems – including the formation of emulsions – gas/liquid systems, solid/liquid systems and solid mixtures. The chapter also outlines the design methods for these different operations, where they exist.

After reading this chapter you should know how to assess mixing quality and understand the mechanisms of mixing in the various operations and regimes described above. You will have encountered methods and correlations to estimate the power requirements for mixing in liquid-based systems. You should also understand the rules governing scale-up of mixing operations: this is particularly important since *ab initio* design methods for mixing processes are, as yet, far from completely developed.

The main emphasis in the chapter is, since this is the area where the science is best developed, on the design and selection of stirred mixing devices for fluids, but you should also understand the basic principles and selection criteria for other types of fluid mixing and for mixing dry or cohesive powders. A key theme of the chapter is the interrelationship between the material properties, the mechanisms of mixing, and the type of unit which is most appropriate for the particular mixing operation.

References and further reading

Bates, R.L., Fondy, P.L. and Corpstein, R.R. (1963) An examination of some geometric parameters of impeller power. *Industrial and Engineering Chemistry, Process Design and Development*, **2**, 310–314.

Bruijn, W., Van't Riet, K. and Smith, J.M. (1974) Power consumption with aerated Rushton turbines. *Transactions of the Institution of Chemical Engineers*, **52**, 88–104.

Calderbank, P.H. (1958) Physical rate processes in industrial fermentation. *Transactions of the Institution of Chemical Engineers*, **36**, 443–463.

Danckwerts, P.V. (1953) The definition and measurement of some characteristics of mixtures. *Applied Scientific Research*, **3**, 279–296.

Donaldson, R. (1985) in *Mixing in the Process Industries* (eds N. Harnby, M.F. Edwards and A.W. Nienow), Butterworth, London, Ch. 15.
Edwards, M.F. (1985) in *Mixing in the Process Industries* (eds N. Harnby, M.F. Edwards and A.W. Nienow), Butterworth, London, Ch. 7.
Edwards, M.F. and Ayazi-Shamlou, P. (1983) in *Low Reynolds Number Flow Heat Exchangers* (ed. Spacek, S), Hemisphere.
Geldart, D. (1973) Types of gas fluidisation. *Powder Technology*, **7**, 285–292.
Greaves, M. and Barigou, M. (1986) Estimation of gas holdup and impeller power in a stirred vessel, in *Fluid Mixing III*, Institution of Chemical Engineers Symposium Series 108, pp. 235–256.
Greaves, M. and Kobbacy, K.A.H. (1981) Power consumption and impeller dispersion efficiency in gas-liquid mixing, in *Fluid Mixing I*, Institution of Chemical Engineers Symposium Series 64, paper L1–L23.
Harnby, N. (1967) A comparison of the performance of industrial solids mixers using segregating materials. *Powder Technology*, **1**, 94–102.
Harnby, N. (1985) in *Mixing in the Process Industries* (eds N. Harnby, M.F. Edwards and A.W. Nienow), Butterworth, London, Ch. 3.
Hoogendorn, C.J. and den Hartog, A.P. (1967) Model studies on mixers in the viscous flow region. *Chemical Engineering Science*, **22**, 1689–1699.
Joshi, J.B., Pandit, A.B. and Sharma, M.M. (1982) Mechanically agitated gas–liquid reactors. *Chemical Engineering Science*, **37**, 813–844.
Kay, J.M. and Nedderman, R.M. (1985) *Fluid Mechanics and Heat Transfer*, Cambridge University Press, Cambridge.
Laufhutte, H.D. and Mersmann, A.B. (1985) Dissipation of power in stirred vessels, in *Proceedings Fifth European Conference on Mixing*, BHRA Fluid Engineering, Cranfield, paper 33, 331–340.
Lee, J.C., Tasakorn, P. and Belghazi, A. (1984) Fundamentals of drop breakage in the formation of liquid-liquid dispersions, in *Proceedings Institution of Chemical Engineers Symposium on Formation of Liquid–Liquid Dispersions*, London.
Mann, R. (1983) Gas–liquid contacting in mixing vessels. Institution of Chemical Engineers Research Fellowship report, Rugby.
McManamey, W.J. (1979) Sauter mean and maximum drop diameters of liquid–liquid dispersions in turbulent agitated vessels at low dispersed phase hold up. *Chemical Engineering Science*, **34**, 432–433.
Metzner, A.B. and Otto, R.E. (1957) Agitation of non-Newtonian fluids. *American Institution of Chemical Engineers Journal*, **3**, 3–10.
Michel, B.J. and Miller, S.A. (1962) Power requirements of gas–liquid agitated systems. *American Institution of Chemical Engineers Journal*, **8**, 262–271.
Middleton, J.C. (1985) in *Mixing in the Process Industries* (eds N. Harnby, M.F. Edwards and A.W. Nienow), Butterworth, London, Ch. 17.
Nagata, S. (1975) *Mixing. Principles and Applications*, Halsted Press, Tokyo.
Nienow, A.W. (1968) Suspension of solid particles in turbine agitated baffled vessels. *Chemical Engineering Science*, **23**, 1453–1459.
Nienow, A.W. (1985) in *Mixing in the Process Industries* (eds N. Harnby, M.F. Edwards and A.W. Nienow), Butterworth, London, Ch. 16.
Nienow, A.W. and Elson, T.P. (1988) Aspects of mixing in rheologically complex fluids. *Chemical Engineering Research and Design*, **66**, 16–21.
Nienow, A.W. and Miles, D. (1968) The effect of impeller/tank configurations on fluid-particle mass transfer. *Chemical Engineering Journal*, **15**, 13–24.
Nienow, A.W., Wisdom, D.J. and Middleton, J.C. (1978) The effect of scale and geometry on flooding, recirculation and power in gassed, stirred vessels, in *Second European Conference on Mixing*, BHRA Fluid Engineering, Cranfield, pp. F1–F16.
Poux, M., Fayolle, P., Bertrand, J. and Bridoux, D. (1991) Powder mixing: some practical rules applied to agitated systems. *Powder Technology*, **68**, 213–234.
Prochazka, J. and Landau, J. (1961) Homogenisation of miscible liquids in the turbulent regime. *Collection of Czech Chemical Communications*, **26**, 2961–2973.
Revill, B.K. (1982) Pumping capacity of disc turbine agitators – a literature review. *Fourth European Conference on Mixing*, BHRA Fluid Engineering, Cranfield, paper R1, 11–24.

Rielly, C.D. and Pandit A.B. (1988) Mixing of Newtonian liquids with large density and viscosity differences in mechanically agitated contactors, in *Sixth European Conference on Mixing*, BHRA Fluid Engineering, Cranfield, pp. 69–71.

Rowe, P.N., Claxton, K.T. and Lewis, J.B. (1965) Heat and Mass transfer from a single sphere in an extensive flowing fluid. *Transactions of the Institution of Chemical Engineers*, **43**, T14–T31.

Smith, J.M. & Warmoeskerken, M.M.C.G. (1986) The dispersion of gases in liquids with turbines, in *Fifth European Conference on Mixing*, BHRA Fluid Engineering, Cranfield, paper 13, 115–126.

Smith, J.M., Middleton, J.C. and van't Riet, K. (1977) in *Second European Conference on Mixing*, BHRA Fluid Engineering, Cranfield, paper F4, 51–66.

Streiff, F.A. (1979) Adapted motionless mixer design, in *Third European Conference on Mixing*, BHRA Fluid Engineering, Cranfield, pp. 171–188.

Uhl, V.W. and Gray, J.B. (1966) *Mixing Theory and Practice*, Vols I and II, Academic Press.

Van Dierendonck, L.L., Fortuin, J.M.H. and Venderbos, D. (1968) The specific contact area in gas–liquid reactors. *Fourth European Conference on Chemical Reactor Engineering*, pp. 205–215.

Van't Riet, K. and Smith, J.M. (1973) *Chemical Engineering Science*, **28**, 1031.

Voit, H. and Mersmann, A.B. (1986) General statement for the minimum stirrer speed during suspension. *German Chemical Engineering*, **9**, 101–106.

Warmoeskerken, M.M.C.G. and Smith, J.M. (1984) The flooding transition with gassed Rushton turbines, in *Fluid Mixing II*, Institution of Chemical Engineers Symposium Series 89, 59–67.

Wilkinson, W.L. and Cliff, M.J. (1977) An investigation into the performance of a static in-line mixer, in *Proceedings Second European Conference on Mixing*, BHRA Fluid Engineering, Cranfield, paper A2–A15.

Zwietering, T.N. (1958) Suspending of solid particles in liquid by agitators. *Chemical Engineering Science*, **8**, 244–253.